HOSTED BY

ELSEVIER

Contents lists available at ScienceDirect

Saudi Journal of Biological Sciences

journal homepage: www.sciencedirect.com

الجمعية السعودية لعلوم الحياة
SAUDI BIOLOGICAL SOCIETY

Original article

Biochemical characterization of immobilized recombinant subtilisin and synthesis and functional characterization of recombinant subtilisin capped silver and zinc oxide nanoparticles

Shreya S. Shettar [a], Zabin K. Bagewadi [a,*], T.M. Yunus Khan [b], Shaik Mohamed Shamsudeen [c], Harsh N. Kolvekar [a]

[a] Department of Biotechnology, KLE Technological University, Hubballi, Karnataka 580031, India
[b] Department of Mechanical Engineering, College of Engineering, King Khalid University, Abha 61421, Saudi Arabia
[c] Department of Diagnostic Dental Science and Oral Biology, College of Dentistry, King Khalid University, Abha 61421, Saudi Arabia

ARTICLE INFO

Keywords:
Recombinant subtilisin
Immobilization
Nanoparticles
Analytical characterization
Biological activities

ABSTRACT

This pioneering research explores the transformative potential of recombinant subtilisin, emphasizing its strategic immobilization and nanoparticle synthesis to elevate both stability and therapeutic efficacy. Achieving an impressive 95.25 % immobilization yield with 3 % alginate composed of sodium along with 0.2 M $CaCl_2$ indicates heightened pH levels and thermal resistance, with optimal action around pH 10 as well as 80 °C temperature. Notably, the Ca-alginate-immobilized subtilisin exhibits exceptional storage longevity and recyclability, affirming its practical viability. Comprehensive analyses of the recombinant subtilisin under diverse conditions underscore its adaptability, reflected in kinetic enhancements with increased V_{max} ($10.7 \pm 15 \times 10^3$ U/mg) and decreased K_m (0.19 ± 0.3 mM) values post-immobilization using N-Suc-F-A-A-F-*p*NA. UV–visible spectroscopy confirms the successful capping of nanoparticles made of Ag and ZnO by recombinant subtilisin, imparting profound antibacterial efficacy against diverse organisms and compelling antioxidant properties. Cytotoxicity was detected against the MCF-7 breast cancer line of cells, exhibiting IC_{50} concentrations at 8.87 as well as 14.52 μg/mL of AgNP as well as ZnONP, correspondingly, indicating promising anticancer potential. Rigorous characterization, including FTIR, SEM-EDS, TGA and AFM robustly validate the properties of the capped nanoparticles. Beyond therapeutic implications, the investigation explores industrial applications, revealing the versatility of recombinant subtilisin in dehairing, blood clot dissolution, biosurfactant activity, and blood stain removal. In summary, this research unfolds the exceptional promise of recombinant subtilisin and its nanoparticles, presenting compelling opportunities for diverse therapeutic applications in medicine. These findings contribute substantively to biotechnology and healthcare and stimulate avenues for further innovation and exploration.

1. Introduction

Subtilisin (EC 3.4.21.14), classified as a serine protease, is present in diverse organisms, including bacteria and plants. Belonging to the S8 clan of proteases, it is recognized for its extensive substrate specificity, enabling it to cleave a diverse array of proteins. These enzymes typically share similar catalytic mechanisms and structural features. Indeed, subtilisin's significance lies in its pivotal role across various industrial applications. Its capacity to hydrolyze proteins effectively and selectively makes it valuable for functions that involve digestion of proteins, cleaning agents, along with the preparation of certain food items. The enzyme's versatility and effectiveness contribute to its widespread use in diverse industrial settings (Schaller et al., 2018). Subtilases, additionally referred to as subtilisins, constitute some of the most varied categories of serine proteases discovered within the genomes of numerous organisms, including viruses. Subtilisins are further split into six separate classes depending on the protein sequence: subtilisins, thermitases, proteinases K, lantibiotic peptidases, kexins, and

* Corresponding author at: Department of Biotechnology, KLE Technological University, Vidyanagar, Hubballi 580 031, India.
E-mail addresses: 01fe21rbt003@kletech.ac.in (S.S. Shettar), zabin@kletech.ac.in (Z.K. Bagewadi), mtatagar@kku.edu.sa (T.M. Yunus Khan), sshahul@kku.edu.sa (S. Mohamed Shamsudeen), 01fe19bbt006@kletech.ac.in (H.N. Kolvekar).

https://doi.org/10.1016/j.sjbs.2024.104009
Received 8 April 2024; Received in revised form 27 April 2024; Accepted 3 May 2024
Available online 4 May 2024

pyrolisins. The subtilisins family has been separated into many subcategories: original subtilisins, exceptionally alkaline proteases, within the cell's proteases, intermediate subtilisins, as well as high-molecular-weight subtilisins. Interestingly, patent research stresses the beneficial effects using subtilisin produced by *Bacillus* sp. across numerous fields. User Serine proteases constitute one of the most extensively studied enzyme classes, featuring two predominant superfamilies: subtilisin-like proteases (SLPs) and trypsins. Both superfamilies share a common catalytic triad (Asp-His-Ser), a structural motif believed to have evolved independently through convergent evolution. The designation "serine proteinases" is attributed to subtilisins and related proteolytic enzymes due to the involvement of the amino acid residue Ser-221 in executing the nucleophilic attack (Bryant et al., 2009; Rozanov et al., 2021). Enzymes retrieved from microbes in surroundings characterized by intense pH levels, conditions of temperature, along with salinity offer tremendous potential for addressing requirements in industry. This is evident in the increasing identification of newly characterized subtilisins showcasing polyextremophilic properties (Mokashe et al., 2018). Beyond that, a research investigated the characterization of new robust subtilisins generated through halotolerant as well as halophilic microbes, given the rising need for innovative biocatalysts in the enzyme market (Falkenberg et al., 2023). Similarly, another study concentrated on building subtilisin proteases, which preferentially destroy the active version of rat sarcoma oncoprotein (RAS) via targeting a conserved location (Chen et al., 2021). These recent references provide insights into various aspects of subtilisin, including its production, versatility, and engineering for specific applications. Several subtilisins and its similar molecules have identical industrial applications. The protease-deficient *B. subtilis* strain WB600 expresses Subtilisin DFE, a fibrinolytic serine proteinase (Peng et al., 2004), which acts as a thrombolytic agent. Other fibrinolytic enzymes like serine protease from *B. subtilis* C10 (Thu et al., 2020) and an enzyme extracted from *B. velezensis* BS2 exhibits strong fibrinolytic activities (Yao et al., 2019). Another discovery of serine proteinase named bafibrinase produced by *Bacillus* sp., revealed to exhibit potential thrombolytic and anticoagulant attributes (Mukherjee et al., 2012). As post-genomic approaches improve, economical microbial medications are increasingly replacing animal-derived pharmaceuticals. The quest for strains expressing proteases with strong fibrinolytic, thrombolytic, as well as anticoagulant capabilities is significant. Bacillus proteinases might be exploited to produce thrombolytic medicines (Danilova and Sharipova, 2020). Keratinolytic bacteria can be an environmentally friendly tool for enhancing sustainable agriculture, agricultural ecosystems, human wellness, soil biology, along with the surroundings. Bacterial keratinases are serine-type proteases with optimal function at pH 6–9 and 30–50 °C (Tamreihao et al., 2019). Varied approaches from molecular biology have been implemented in addition to standard strategies for screening bacteria carrying unique and fascinating proteases from varied environments. Metagenomic assessment, directed evolution, and site-directed mutations are instances of such techniques that have been employed to alter or design various proteases with enhanced or unique properties. In addition to these resource-intensive methodologies, the process of genome sequencing and automated annotation contributes potential sequences to the swiftly expanding online database. This introduces a complementary approach to picking protease genomes suited for commercial applications (Falkenberg et al., 2022).

Immobilization is an important technique in various fields, offering several advantages and employing different approaches. Because immobilized enzyme systems are heterogeneous, they enable for facile recovery of the two enzymes and products, numerous enzyme reuses, perpetual operation of processes involving enzymes, instantaneous dismissal, and improved adaptability in fermenter architectures. Immobilizing enzymes or proteins shields them against adverse conditions in the environment, for instance rising temperatures in addition to excessive pH numbers, enhancing their stability and life expectancy. Even with minimal enzyme loading, the outcomes of binding the protease onto support material under circumstances involving quick or gradual immobilization should produce a completely different outcome. However, at lower immobilization efficiency circumstances, the enzyme is able to circulate in the particle's porosity prior to becoming immobilized. This manner, enzyme will eventually spread on the backing surface, offering a greater proportion of the enzyme's active components rather than when the enzyme immobilizes so rapidly that the enzyme molecules become compressed together, producing a crown at the very start of the supporting openings (Tacias-Pascacio et al., 2021). Moreover, immobilization enables the use of enzymes and other sensitive compounds that are otherwise untenable due to their instability under certain factors like pH, temperature, and organic solvents (Hassan et al., 2019). Enzyme immobilization approach effectively inactivates water-soluble enzymes. Enzyme confinement refers to an aspect (matrix/support) that is distinct from the ones found in substrates and products. Enzyme covalent immobilization with solid support assists in ensuring proteins align properly by interacting to specific amino acid sites. Compared to previous immobilization approaches, this enables for more precise protein arrangement. Covalent immobilization involves functional structures that attach enzymes to water-insoluble carriers, preserving their respective effective conformation and location (Mohammadi et al., 2015; Wahba and Hassan, 2017). The utilization of an immobilized enzyme may not always be necessary, aside from meeting economic requirements in the process. Starting out, the expenditure of enzymes were incongruent with the single-cycle utilization of digestive enzymes, necessitating the introduction of heterogeneous biological catalysts to permit enzyme regeneration and render the technique profitable (Bolivar et al., 2022). Immobilization procedures are largely organized into two distinct groups: physically and chemically based approaches. Physical techniques are distinguished by the presence of mild monovalent connections such as bonding of hydrogen, van der Waals pressures, hydrophobic relations, specificity binding, ionic adherence, or mechanical confinement of the enzyme within the structure of support. Chemical approaches entail the formation of covalent connections involving the enzyme's structure alongside the backing substance through ether, thioether ether, amide, or carbamate interactions. Adsorption, covalent binding, entrapment, encapsulation, and cross-linking are the five main strategies for immobilizing enzymes (Brena et al., 2013; Hassan et al., 2019; Wahba and Hassan, 2017). Entrapment by sodium alginate is one of the feasible methods. The gelation mechanism involves an ionic exchange process in which the sodium within the alginate undergoes exchange with calcium II present in the gelling medium. This exchange leads to the creation of linkages between linear chains, originating in to the creation of an insoluble gelatin featuring a form that is spherical. Only the G-blocks in alginate are thought to engage during intermolecular communication with cations that are divalent, such as Ca^{2+}, during hydrogel formation. The physical characteristics of hydrogels are heavily influenced by the M/G ratio, G-block size, a sequence, and molecular composition of the polymer (George and Abraham, 2006). Alginate's discovery has led to significant research and advancement of its use for immobilization (Mohd Hussin et al., 2020). The stability of the enzyme can be enhanced without any activity loss through enzyme entrapment since there does not exist chemical connection amongst the enzyme and the base substance. In this approach, the crucial component is choosing of the supporting substance along with the size of pores, both of which have an impact on the relationships that occur within the enclosed enzyme and the substrate that is employed in the process. The advantage of this technique is that the enzyme freely moves inside the support carrier. The entrapment technique offers a range of benefits, such as a high capacity for loading enzymes, cost-effectiveness in fabrication, improved mechanical stability of entrapped enzymes, along with reduced transfer of mass limitations. Additionally, it provides the flexibility to modify the encapsulation component to achieve an optimal microenvironment, ensuring the desired pH, polarity, or amphiphilicity (Costa et al., 2004; Maghraby et al., 2023; Mohamad et al., 2015). Immobilization

facilitates the increase of enzyme properties which include action, reduction of suppression due to the byproducts of reaction and metallic ions, equilibrium, and specificity toward the substrate. Additionally, immobilization can inhibit constituent disengagement in multimeric enzymes.

Nanomaterials play a crucial role in addressing significant challenges. The term "nanomaterial" pertains to a size on the scale of a trillionth of a meter, commonly referred to as a nanometer. Nanomaterials find extensive applications in environmental monitoring, biomedicine, pharmaceuticals, optoelectronics, textile industry and cosmetics. These small nanoparticles affect their physical properties in a variety of ways, such as boosting their volume-to-surface-area proportion and influencing particle size through quantum features (Naseem and Durrani, 2021). In contemporary advanced materials, the aspect, dimensions, and configuration in the synthesis of metal nanoparticles hold considerable significance. Nanoscale metal oxides exhibit numerous exceptional properties, like extended removal capacity and selectivity for heavy metals. They have tremendous promise as prospective heavy metal adsorbents. Metal oxide-based nanoparticles encompass oxides of manganese, nanosized iron, titanium, cerium, zinc, magnesium, aluminum, and zirconium (Dreaden et al., 2012; Gehrke et al., 2015). The encapsulating agent is a molecule with amphiphilic characteristics, consisting of a head group that is polar with a non-polar in nature hydrocarbon end. As a result of its amphiphilic character, these substances impart functioning along with enhanced interoperability with an additional phase. Various categories of encapsulating agents have been utilized in the generation of nanoparticles, encompassing surfactants, diminutive ligands, polymers, dendrimers, cyclodextrins, and polysaccharides (Radini et al., 2018). In the creation of nanoparticles, the inclusion of capping or stabilizing agents is imperative to augment their biomedical efficacy. This is accomplished by diminishing the toxic effect simultaneously boosting their biological suitability in addition to bioavailability amongst cells that are alive. These compounds serve a significant function in averting the formation involving groupings of nanoparticles, enhancing their colloidal stability, and regulating the uncontrolled expansion of nanoparticles, notably in the instance of metallic and oxides of metal nanomaterials. Closely examined for their applications in biomedicine, capped nanoparticles have garnered significant attention, particularly for their roles in antimicrobial, antioxidant, anticancer, and antidiabetic activities (Hola et al., 2015). Magnetic nanoparticles (MNPs) exhibit superparamagnetism, a size-dependent feature helpful for manipulating them with an external magnetic field. When the magnetic field is removed, these particles lose their residual magnetism. This property has led to the creation of biomolecule-nanoparticle (bio-NP) hybrids that are utilized in biological applications such as disease diagnostics and therapy (Masi et al., 2018). Previous studies have indicated that nanoparticle-based antimicrobial formulations could serve as a potent antibacterial agent. Based on the discoveries made, it can be asserted that the antimicrobial properties of nanoparticles are solely contingent on their physical characteristics. This involves the adhesion of nanostructures onto the structure of the cell barrier, their association with it, including the denatured state of the cell exterior proteins. As a result, these actions create permeable membranes and substantially alter the internal makeup of the membrane of a cell. Ultimately, it improves the porousness of the cellular membrane, which facilitates the passage of extracellular fluids into the cell (Zhai et al., 2017). Numerous nano-enabled methods are proposed to advance yields of crops and support the essential rise of supplies for nourishment, livestock, and fuels while adhering to sustainable agriculture. Nanoparticles are regarded as "magic-bullets" for improving agricultural efficiency as they include nutrients, essential genes, and naturally occurring compounds that may be adjusted to specific plant structures or locations (Bamal et al., 2021). As previously described by (Milanezi et al., 2019), gold that were attached (Au) nanoparticles undergo surface functionalization via the encapsulation with quercetin, with the purpose of augmenting the accessibility associated with the molecule and, subsequently, its antioxidant activity. The antioxidant activity of quercetin capped with gold nanoparticles is assessed through nitric oxide (NO), 2,2-diphenyl-1-picrylhydrazyl (DPPH), and 2,2′-azino-bis (3-ethylbenzothiazoline-6-sulfonic acid) (ABTS) free radical scavenging assays. This phenomenon can be ascribed to the modifications in the surface topology and nanoparticle size significantly contributing to the enhancement of their biological properties. Antioxidants neutralize free radicals that produce oxygen compounds that are reactive (ROS), including nitric oxide (NO), radicals of hydroxyl (OH^-), and superoxide anion (O_2^-), acting as a defensive mechanism in healthy organisms (Bedlovičová et al., 2020; Javed et al., 2020). Metal or metal oxide nanoparticles derived from plant sources exhibit notable effects on various cancer cell lines, including but not limited to Hela, Hep 2, and HCT 116 cell lines. The silver nanoparticles synthesized through biological means-initiated alterations in the cell cycle and enzymes within the bloodstream. Additionally, nanoparticles govern the generation of radicals that are free within the cell's membrane. Typically, radicals that are unstable are responsible for the acceleration of cell growth and the impairment of how cells normally operate. The controlled presence of gold nanoparticles induces the apoptosis mechanism in tumor cells (malignant cells). The incorporation of nanoparticles made of metals and metal oxides in medical science has shown usefulness in identifying and treating various kinds of cancer cells (Akhtar et al., 2013; Bukhari et al., 2021; Das et al., 2013).

Furthermore, there exists a dearth of transparency on the biochemical features associated with unbound and immobilized recombinant subtilisin, particularly when it comes to immobilization method involving purified recombinant protein, as explored in the current study. From an economic standpoint, the unfettered recombinant subtilisin is costly, but opting for the immobilization of recombinant subtilisin using alginate was chosen for its straightforward retrieval, simplicity, cost-effectiveness, and the absence of chemical waste generation. The impact of specific factors on the immobilization process, such as various surfactants, organic solvents, inhibitors and detergents of the alginate-subtilisin beads, were also investigated. Nanoparticles composed of Ag and ZnO, coupled with recombinant subtilisin under capping, underwent synthesis and biological assessment, encompassing evaluations of their antibacterial, antioxidative, and cytotoxic properties. The encapsulated nanostructures have been further investigated by deploying the Fourier transform of infrared spectroscopy (FTIR), thermogravimetric analysis (TGA), atomic force microscopy (AFM) and scanning electron microscopy (SEM) combined with energy dispersive X-ray spectroscopy (EDS). The current investigation has unveiled noteworthy and impressive immobilization studies and assessment, biological activities, as well as the behavior of nanoparticles in the presence of purified recombinant subtilisin. This prompts further exploration of its potential applications in the healthcare sector.

2. Materials and methods

2.1. Chemicals and microbial cultures

The ingredients administered in this current study were procured from Sigma-Aldrich Pvt Ltd. (USA) and Merck and Co. Inc. (USA). The test organisms deployed in the antibacterial investigations, including *Pseudomonas aeruginosa* (MTCC 2297), a strain of *Salmonella typhimurium* (MTCC 98), bacterium *Bacillus licheniformis* (MTCC 429T), a strain of *Bacillus cereus* (NCIM 2217), the *Escherichia coli* strain (MTCC 443), and the bacterium *Staphylococcus aureus* (MTCC 737), have been procured from two sources: the National Collection of Industrial Microorganisms (NCIM), Pune, and the Microbial Type Culture Collection and Gene Bank (MTCC), Chandigarh. Furthermore, cytotoxic examinations have been conducted utilizing the cell lines of MCF-7 breast cancer. Goat hide and sheep blood were obtained from a local butcher shop. A subtilisin gene optimized for codon usage was synthetically created based on the identified *Bacillus subtilis* sequence. The gene was effectively

introduced into *E. coli* DH5α cells, followed by induction for robust expression at high levels in *E. coli* BL21 (DE3). The findings of the previous study contributed to advancing the development of a highly efficient purified recombinant subtilisin to be assessed for its biochemical characterization, immobilization kinetics and synthesis of nanoparticles and its bioanalytical characterization in the current study (Shettar et al., 2023b).

2.2. Protease (Casein) assay

Casein assay was assessed by measuring the liberation of free tyrosine residues through the hydrolysis of casein. A formulation which included 0.5 mL about completely processed recombinant subtilisin in addition to 0.5 mL of casein protein powder (around a dosage of 10 mg/mL) was made up using glycine-NaOH solution (with a pH 10, at 100 mM dosage). The combination was subsequently left to incubate about a ten-minute period at 80 °C. The reaction had been inhibited with the incorporation comprising 2.5 mL holding a solution with a concentration of 10 % of trichloroacetic acid (TCA), while maintaining the solution intact for 30 min at ambient temperature. To extract the precipitate, the combined product was spun down for fifteen minutes at 10,000 revolutions per minute (rpm). 0.5 mL from the translucent supernatant had been combined into 2.5 mL sodium carbonate in addition to 0.5 mL Folin-Ciocalteu's phenolic ingredient, pursued by additional incubation at the temperature of the room over 30 min. The absorption coefficient at 660 nm was taken into account employing a spectrophotometer equipped with an UV–Vis. The minimal quantity of subtilisin performance is a portion of the enzyme whose services emits 1 μM of tyrosine (an amino acid) each minute under the right circumstances for testing (Mechri et al., 2021; Muhammed et al., 2021).

2.3. Subtilisin assay

The chemical-based peptide (N-Suc-F-A-A-F-*p*NA) (track code S2628, Sigma Aldrich) was utilized for the assessment of subtilisin activity. To start the chemical process, a 200 μL combination containing enzyme suspension of 30 μL, 30 μL comprising of the chromogenic peptide, together with 140 μL 20 mM Tris-HCl (pH 7.4) was left to react around 37 °C over 30 min. The quantity of emitted p-nitroaniline was assessed using spectrophotometry that measures ultraviolet light at an emission wavelength of 405 nm. Under typical laboratory settings, a single enzymatic reaction on a chemically synthesized peptide may be characterized as a particular quantity of digestive enzyme that yields 1 μmol about p-nitroaniline every minute (Couto et al., 2022; Shettar et al., 2023a).

2.4. Protein quantitation

The BCA protein detection pack was implemented to determine the overall unbound protein quantity (in milligrams) containing subtilisin, utilizing conventional bovine serum albumin (BSA) as a baseline. The examination had been executed in threefold followed by outcomes offered in the form of mean concentration (mg/mL) ± variance by standard deviation (Bagewadi et al., 2017; Shettar et al., 2023a).

2.5. Immobilization of recombinant subtilisin

2.5.1. Sodium alginate entrapment method

The beads' consistency was investigated using sodium alginate immobilization. 3 g of sodium alginate were solubilized in distilled water (100 mL) to generate 3 % solution. One mL of processed recombinant subtilisin was appended to ten mL of ready sodium alginate solution and the tube has been flipped two to four times to ensure uniform dispersion. To that aim, the subtilisin and carrier combination was progressively dispensed from a height of ~15 cm with a 10 mL syringe into a chilled solidifying buffer of 0.2 M calcium chloride while stirring on a magnetic motor. The newly formed beads received a treatment to a curing procedure inside a refrigerator at 4 °C for an uninterrupted period of an hour. The solidified beads thus produced underwent two to three wash cycles with distilled water that is sterile and were then preserved at 4 °C in distilled water, until required. All experimental procedures were executed with aseptic precision within a laminar flow hood (Nadeem et al., 2020). The Ca-alginate beads with immobilized recombinant subtilisin were evaluated for the percentage of immobilization yield using the following equation (1):

$$\text{Immobilization yield } \% = \left(\frac{\text{Catalytic activity immobilized subtilisin}}{\text{Catalytic activity of free subtilisin}}\right) \times 100 \quad (1)$$

2.6. Biochemical analysis of pure genetically modified subtilisin, including free and immobilized

2.6.1. Investigation of the ideal pH, temperature, as well as durability of immobilized subtilisin

The examination encompassed the exploration of the influence of pH levels, various temperature and amount of substrate on the subtilisin functionalities of immobilized subtilisin. The assessment of optimum pH, temperature and its stability for free recombinant subtilisin was studied and reported previously (Shettar et al., 2023b). To investigate the consequences regarding the pH level on subtilisin effectiveness and stability, the experiment mix was subjected to incubation for 30 min across a spectrum of various buffers, encompassing a pH range of 3–12, containing casein as a substrate (Shettar et al., 2023b). The buffering agents employed included a buffer made of acetate (with a pH 3–5), sodium a buffer consisting of sodium phosphate (pH level 6–8), in addition to glycine-NaOH solution (pH range: 9–12). The durability of immobilized subtilisin under different pH conditions had been assessed by subjecting it to incubation for 20 h at pH 9,10 and 11 and 35 °C. Portions were taken at constant 2-hour intervals, along with the remaining subtilisin activities was determined and transmitted as the relative subtilisin activities (Mechri et al., 2022).

The most suitable temperature for the encapsulated subtilisin has been identified through an acceptable temperature range between 30–90 °C pursuant to a pH of ten (using glycine-NaOH buffer) and in presence of 2 mM Ca^{2+} over a 30-minute duration with casein as the substrate. The effectiveness of subtilisin in the absence of any sort of additive was adopted as a measure of control. The thermal endurance of immobilized subtilisin was evaluated over frequent 2-hour frequencies for its relative activity, treating it to temperatures that varied between 65 and 85 °C throughout a 20-hour timeframe (Qamar et al., 2020).

2.6.2. Storage and reutilization of immobilized subtilisin

The stability during storability of unbound subtilisin and calcium alginate immobilized subtilisin beads were examined at temperatures of 4 °C and ambient temperature (25–27 °C). The remaining activities of the sample were measured periodically over a duration of 2 months with 15 d interval.

By recovering the sodium alginate immobilized subtilisin beads throughout numerous cycles, the working durability of the immobilized subtilisin was reviewed. During the recycling process, the beads were rinsed using water that had been deionized in order to eliminate superfluous substrate as well as leftover reaction byproducts. The rejuvenated subtilisin beads, whether encapsulated, were then utilized in the subsequent cycle. A fresh preparation of the substrate was made on each cycle. The encapsulated subtilisin beads' original enzyme function was estimated to be 100 % (Mechri et al., 2022; Sattar et al., 2018).

2.6.3. Utilizing free and immobilized recombinant subtilisin for surfactant, metal ion, additives, and organic solvent determination

For the purpose of investigating the consequences of surfactants

(Tween 40, Tween 80, Triton X-100, the peroxide form of hydrogen, along with Sodium Dodecyl Sulphate) of a concentration of 1 % affecting the durability of unbound and immobilized subtilisin, the sample was pre-incubated with each surfactant lasting 30 min. Subsequently, a subtilisin assay was assessed ensuing the previously described procedure (Muhammed et al., 2021).

To investigate the implications of multiple metal ions on the functioning of the two types of independent and immobilized subtilisin, metallic ions (ferrous sulfate, magnesium sulfate, sodium chloride, potassium chloride, calcium chloride, zinc sulfate, copper sulfate) were introduced to the enzyme at a dosage of 0.5 M and incubated for 30 min. The relative activities were measures using subtilisin assay (Bhatt and Singh, 2020).

To investigate the impression of additives on both unbound and immobilized subtilisin, the sample was pre-incubated with 1 M concentrations of DTT, PMSF, β-mercaptoethanol, and EDTA for 30 min. The relative activity was then calculated through the casein assay (Yang et al., 2020). The control was termed as untreated.

To look into the implications of solvents that are organic upon subtilisin action, the recombinant subtilisin had been pre-incubated over a period of thirty minutes containing 10 % by volume of the following solvents: ethyl acetate, ethanol, methanol, chloroform, glycerol, alongside benzene. The relative efficiencies were computed, with the activity of the control set as 100 % (Bhatt and Singh, 2020). The subtilisin manipulations have been administered in triple quantities, and the outcome data is shown as the average ± deviation from the norm.

2.6.4. Effect of substrate specificity on immobilized recombinant subtilisin beads

The hydrolytic capability of calcium alginate immobilized recombinant subtilisin was quantified according to conventional conditions for testing by employing an assortment of substrates, the protein casein (normal), azo-casein (improved), N-acetyl-L-tyrosine ethyl ester monohydrate (ATEE), N-benzoyl-L-tyrosine ethyl ester (BTEE) (esters), alongside a synthetic peptide such as N-Suc-F-A-A-F-*p*NA. The substrate specificity of free recombinant subtilisin has been reported earlier (Shettar et al., 2023b). The interactions of recombinant subtilisin with each of the substrates were carried out using the established conventional assay practice outlined earlier (Mechri et al., 2022). In the scenario of the azo-casein base, determining a single molecule of subtilisin performance entailed the capability of the enzyme to catalyze the hydrolysis of azo-casein, culminating in a noticeable 0.01 increase in the absorbance coefficient pursuant to the prescribed test environment. For synthetic peptide, refer section 2.3 to calculate the subtilisin assay. In the context of the BTEE substrate, a single instance of subtilisin functionality (either esterase or amidase) has been described as that of a particular amount of enzyme that results in an alteration in absorbency at a rate of 0.001 every minute given normal testing parameters (Shettar et al., 2023b).

2.6.5. Kinetics of calcium alginate immobilized subtilisin

The kinetics, which include the Michaelis-Menten ratio (K_m), the highest velocity (V_{max}), turnover number (k_{cat}), and k_{cat}/K_m, have been estimated applying the Lineweaver-Burk diagram using the suggested equation (Kerouaz et al., 2021). Kinetic parameters for the free recombinant subtilisin using casein and synthetic substrate has been reported previously by Shettar et al., (2023b). Kinematic coefficients were established making use of the casein protein along with synthetic peptide as bases at doses ranging from 0.1 to 10 mM based on normal experiment protocols.

The turnover number (k_{cat}) was determined utilizing the subsequent equation:

$$k_{cat} = \frac{V_{max}}{[E]} \quad (2)$$

where [E] reflects the level of enzyme concentration that is active whereas V_{max} marks the absolute maximum velocity.

2.7. Biosynthesis of silver and oxide of zinc nanoparticles employing recombinant subtilisin alongside UV–Vis spectroscopic analysis

Silver nitrate preparations having dosages of 5 mM, 10 mM, as well as 50 mM were meticulously created under perpetual stirring on a stirrer with a magnetic field. For each concentration, a combination of 0.5 mL of undiluted recombinant subtilisin plus 4.5 mL of a solution containing silver nitrate was generated then underwent incubation throughout the surrounding temperature over a period of thirty minutes whilst being exposed to UV light. Subsequently, the mixture underwent microwave heating for a duration of 30 s to observe for a difference of color from colorless to brown denoting the presence of nanoparticles generated. The ultraviolet (UV)-visible spectroscopy approach was implemented to establish the wavelength associated with the silver nanoparticle (AgNP) solution. The harvested AgNP were segregated through spinning at a speed of 10,000 revolutions per minute for a span of 10 min to eliminate the unbound metals and subsequently desiccated for further characterization. The silver nanoparticles obtained in this manner were capped with recombinant subtilisin and, consequently, referred to as "subtilisin-capped AgNP". This method was previously explained by Sidhu and Nehra (2021).

Subtilisin-capped zinc oxide nanoparticles (ZnONP) were generated employing recombinant subtilisin in a reaction according to the technique explained by Jeyabharathi et al., 2022, which included the amalgamation of 10 mM zinc acetate dihydrate (700 µL) plus 300 µL containing recombinant subtilisin. The reaction underwent incubation at 55 °C for a duration of 15 min, succeeded by an additional period of incubation at room temperature for 4 h. At regular intervals, portions of the reaction solution were withdrawn and analyzed using UV–Visible spectroscopy to measure the surface plasmon resonance during the synthesis of ZnONP. The sediment was harvested through centrifugation at 15,000 revolutions per minute for a 15 min span, and subjected to two washes with deionized water. Following this, ethanol was used for an additional wash to eliminate any organic residues. The collected sediment subsequently airflow-dried inside a blast of air oven around 50 °C until 20–24 h before being stored for sequential evaluation. Thus, both the subtilisin-capped nanoparticles were utilized for further functional and analytical characterizations.

2.8. Characterizing the functionality of nanoparticles capped with recombinant subtilisin

2.8.1. Assessing antibacterial activity (AMA) along with determining minimal inhibitory concentration (MIC) utilizing nanoparticles capped with recombinant subtilisin

The well-known agar well diffusion approach had been utilized to examine the antibacterial response of recombinant subtilisin encapsulated nanomaterials (Ag and ZnO) in order to minimize the growth of the two types of bacterial test strains (Sidhu and Nehra, 2021). Pathogenic test strains utilized in this experiment were *B. cereus, S. aureus* and *B. licheniformis* (Gram positive) and *S. typhimurium, E. coli* and *P. aeruginosa* (Gram negative). The pathogenic varieties were raised 18–24 h in Luria Broth (LB), and on the subsequent day, each freshly developed culture (100 µl) was evenly disseminated on a plate containing Luria Agar (LA). Wells in the aforementioned plates were punched utilizing a sterile well borer (6 mm) for the inclusion of the test solutions of recombinant subtilisin bound AgNP and ZnONP. Following an overnight incubation at 37 °C in upright locale, the extent of the inhibition zone width, which extends outward transversely around the wells, was measured. The positive control used was cefixime at a dosage level of 5 µg/mL.

MIC is characterized as the smallest quantity of the sample to be tested, required to impede the development of the targeted

microorganisms. MIC value shows an inverse correlation with the effectiveness against microbes; the greater the MIC, the weaker the antimicrobial efficacy. To analyze the inhibitory concentration (MIC) of recombinant subtilisin bound AgNP as well as ZnONP at 50 mM each, microbroth dilution approach was implemented, adopting the recommendations specified as per the Institute for Clinical and Laboratory Standards (CLSI). To achieve the rapid development stage, test microorganisms were cultured in Mueller-Hinton medium then retained at night in 37 °C with steady rotation at 150 revolutions per minute. In order to obtain an appropriate cell count (10^7 CFU/mL), the incubated cells were diluted. Diverse sample concentrations of recombinant subtilisin bound AgNP and ZnONP were added to the culture media and underwent incubation for a period of 24 h at 37 °C temperature. The wavelength at 600 nm spectrophotometrically measured the turbidity which demonstrated the inhibitory effect of all the samples on the test pathogens. The negative control comprises culture broths that have not been infected, whereas the positive control contains culture broths that have not had any samples incorporated into them (Bagewadi et al., 2019; Shettar et al., 2023a).

2.8.2. Antioxidant activity of recombinant subtilisin capped nanoparticles

2.8.2.1. Assessment of α, α-Diphenyl-β-picryl-hydroxyl (DPPH) radical scavenging property. The free radical scavenging evaluations for recombinant subtilisin conjugated nanoparticles of silver (AgNP) at a concentration of 50 mM and nanoparticles of zinc oxide (ZnONP) with a concentration of 50 mM were carried out utilizing the approach that was followed by Alahdal et al. (2022). Briefly, each sample (AgNP and ZnONP) at concentrations spanning 5–50 mM underwent a reaction with freshly prepared 1 mL of 0.135 mM DPPH (reinforced in methanol). The incubation occurred at 25 °C in darkness for a period of 30 min. A spectrophotometer equipped with an UV–Vis was deployed to determine the wavelength absorbed throughout the chemical reaction, whose wavelength was 517 nm. The percentage of scavenging activity was then computed by equation (3), with ascorbic acid at a concentration of 1 mM serving as the standard.

$$\text{Scavenging activity } (\%) = \left(\frac{\text{Ac} - \text{As}}{\text{Ac}}\right) \times 100 \quad (3)$$

where (Ac) corresponds the absorbance of control, and (As) denotes absorbance corresponding to sample.

2.8.2.2. Assessment of 2,2-azino-bis-3-ethylenebenzothiozoline-6-sulfonic acid (ABTS) activity. The previously published approach was utilized to investigate the ABTS-scavenging efficiency of recombinant subtilisin bound AgNP (50 mM) as well as ZnONP (50 mM) (Ashokbhai et al., 2022). In the absence of light, the reaction that occurred involving ABTS along with the potassium persulfate solution took 16 h and yielded an optical density equal 0.70 at about 734 nm. 0.5 mL of the two samples (AgNP and ZnONP) had been combined along with 2 mL of ABTS to yield an aggregate quantity of 2.5 mL. This mixture was left to develop at 25 °C until 30 min. The wavelength of light absorbed via the chemical process was subsequently measured at 734 nm. The capability to scavenge was determined for each respective sample over a timeframe ranging from 12 to 60 h. The benchmark for this assessment was Butylated hydroxytoluene (BHT) (Shettar et al., 2023a).

2.8.3. Assessing of anticancer effects by 3-(4, 5-dimethylthiazol2-yl)-2,5-diphenyltetrazolium bromide (MTT) assay utilizing recombinant subtilisin-capped nanoparticles

The MTT technique was applied to evaluate the *in vitro* cytotoxicity of recombinant subtilisin-capped nanoparticles (Ag and ZnO) upon breast cancer cells derived from humans MCF-7 line of cells. To accomplish this, a 96-well microplate was employed, and 5000 cell/well of cancer cell lines were sown and incubated for an impressive 24-hour duration. To address the cells, diverse concentrations of subtilisin bounded by AgNP and ZnONP were employed over a 48-hour period. The concentration range spanned from 3.125 to 100 μg/mL. Following the treatment, the medium had been removed and the cells went through washing utilizing a solution of PBS, which stands for phosphate-buffered saline. The cultured cells received treatment for a total of four hours by MTT (0.5 mg/mL) inserted into every single well. A dimethyl sulfoxide (also known as DMSO) solution had been employed for scattering the newly generated formazen granules while the absorbance spectra at 570 nm had been determined employing a microplate reader with make of BioTek Epoch 2. The treated cancerous cells those weren't exposed to any chemicals had been designated as the control group, exhibiting 100 % survival of the cells. The absorption frequency of the cells that were treated were then correlated in order to determine the cell's longevity, whereas doxorubicin served as the reference medication. All experiments were conducted three times (P et al., 2021).

2.9. Analytical characterization

2.9.1. HPLC analysis of recombinant subtilisin

The HPLC analysis involved examining 10 μL of the purified recombinant subtilisin using a column with 150 mm × 4.6 mm dimensions, and a of 4 μm (particle size) (Agilent Technologies High-performance liquid chromatography 1260 Infinity II). A variable wavelength detector (VWD) tuned to 250 nm was employed for detection. The samples underwent separation through a multistep linear-gradient method using methanol, along with distilled water (70:30, v/v) as solvents. The separation occurred under an average flow speed of 0.5 mL every minute with a pressure range of 0–400 bar throughout a 30-minute period (P et al., 2021).

2.9.2. FTIR detection of recombinant subtilisin capped nanoparticles

Infrared spectroscopy using the Fourier transform (FTIR) was conducted by employing the FTIR Spectrometer Nicolet, 5700 in order to investigate the spectrum of wavelengths that exhibit the nature of chemical connections along with probable groups with functional properties identified in nanoparticles made of Ag and ZnO. Utilizing the potassium bromide (KBr) technique, the samples were compacted and grounded to pellets, and used for analysis. A spectral range spanning 4000 to 400 cm^{-1} was employed, with a resolution set at 1.0 cm^{-1} (Jeyabharathi et al., 2022).

2.9.3. SEM with EDS evaluation of recombinant subtilisin capped nanoparticles

SEM-EDS (JEOL manufacture, JSM-IT500L) furnishes information regarding the exterior morphological characteristics, construction, chemical content, including orientation of the material being examined. The dehydrated samples were subjected to an electron beam, yielding the image and size information of AgNP and ZnONP (Bagewadi et al., 2020a; S. Ibrahim et al., 2021).

2.9.4. TGA of recombinant subtilisin coated nanoparticles made of Ag and ZnO

TGA was performed on recombinant subtilisin bounded by AgNP and ZnONP to determine their thermal stability employing an SDT-Q600 equipment. The crushed nanoparticle specimen underwent heating in a nitrogen-controlled chamber at an average rate of 10 °C per minute, with temperatures fluctuating between 25 and 800 °C (Bagewadi et al., 2020b; Shettar et al., 2023a).

2.9.5. AFM of recombinant subtilisin capped nanoparticles

The topical forms and configurations of the two capped nanoparticles had been investigated by the application of AFM by Nanosurf, Switzerland. A transparent slide had been coated with a 10 μL droplet containing AgNP and ZnONP nanoparticles, resulting in a fine layer. Following a brief drying in the air, the outermost layer of the specimen

was inspected employing the piezoelectric detector for imaging. The object being studied was thereafter scanned through contact mode utilizing a silicon nitride cantilever to thoroughly probe the surface. The obtained microscopic pictures were examined using the Easyscan 2 program (Guilger-Casagrande et al., 2021).

2.10. Applications of recombinant subtilisin

2.10.1. Biosurfactant assay by oil spreading method

The purified recombinant subtilisin was examined for biosurfactant activity through oil spreading assay that provides insights into the surfactant's capability to curtail the surface tension of water and enhance its interaction with hydrophobic substances like oil. A giant petri tray (9 cm diameter) was filled with 50 mL of distilled water, then added 25 μL with mineral oil. A volume of ten microliters from the recombinant subtilisin was applied to the mineral oil surface, and the extent of mineral oil displacement by the protein was quantified. Water was used as control. The oil spreading area (cm^2) was determined. (Adetunji and Olaniran, 2021; Zobaer et al., 2023).

2.10.2. Keratinolytic activities in dehairing of goat hide

Goat hide was procured from the nearby market and appropriately cleansed using distilled water. Small sections of the hide (3 × 3 cm^2) were submerged in the recombinant subtilisin and subjected to incubation inside an incubator with shaking condition at 40 °C at 150 rpm for a duration from 4 to 24 h. A small section of hide was also treated with 1 % Na_2S as a chemical treatment while control was goat hide in buffer. Similar incubation was carried out for all the samples. Following incubation, the individual parts were soaked in distilled water to get rid of excess loosened hair. Throughout the operation, the depilation technique was examined by assessing factors that included color, overall appearance of the leather, and duration for easy hair removal from the hide post treatment was estimated (Li et al., 2022; Sarkar and K, 2020).

2.10.3. Blood stain removal

The recombinant subtilisin's capacity to eliminate stains was assessed on 4 cm × 4 cm strips of white cloth made of cotton. These fabric fragments were uniformly dyed using 0.5 mL of blood from an animal, let to air dry over 18 h, after which they were washed with water that had been distilled to eliminate the extra blood. The fabric pieces were once more left to air dry and then exposed to various washing treatments. A cloth with blood stain was washed with water and set as control. A stained fabric section received treatment from a regional laundry detergent lacking any intrinsic enzymes. Another piece underwent application of the subtilisin utilized in this investigation. Ultimately, a single among the stained fabric sections had been cleaned utilizing a blend containing detergent and subtilisin. Every single of the aforementioned cleansing techniques had to be conducted under 40 °C for 15 min, then finished with drying in the air. The fabric samples were visually examined to determine the effectiveness of stain elimination. The untouched soiled cloth portion acted as the control (Hadjidj et al., 2018; Matkawala et al., 2019).

2.10.4. Dissolution of blood clot

Sheep blood (0.5 mL) was obtained from local butcher store and placed in centrifuge tubes. The addition of recombinant subtilisin as test and distilled water as control was done to two different tubes with blood. and the clot lysis was examined. Using a constant incubation period of 4 h, the effectiveness of subtilisin was investigated following the blood clot dissolution assay protocol. Upon a four-hour period of incubation at 37 °C, the percentage of the total weight dissociation of blood clots had been analyzed for the samples being tested. Following spinning the tubes at 20,000 rpm for a duration of fifteen minutes, the centrifuge tubes and blood clot (pellet) were weighed (Li et al., 2021; Sharma et al., 2019). The clot dissolution rate was evaluated as follows:

$$\text{Clot dissolution rate} = \frac{\text{clot weight prior dissolution} - \text{clot weight post dissolution}}{\text{clot weight prior dissolution}} \times 100\% \quad (4)$$

2.11. Statistical analysis

All assessments were conducted with three independent replicates. The mean plus standard deviation of repeated determinations served to illustrate the outcomes of the experiment. Observations were deemed to be statistically noteworthy with a value of P that were below or in the range of 0.05.

3. Results

3.1. Characterization of immobilized recombinant subtilisin

3.1.1. Recombinant subtilisin entrapment in calcium alginate beads

As reported previously by Shettar et al., (2023b), the recombinant subtilisin was expressed within the bacterium E. coli DH5α cells then extracted through the technique of affinity chromatography, yielding 179 U/mL of subtilisin activity. This purified recombinant subtilisin was used for further assessment and characterization starting with immobilization using sodium alginate method by entrapment technique. The immobilization with Ca-alginate presents numerous advantages due to its cost-effectiveness and environmentally sustainable properties. The gel formation substance, Na-alginate, can be employed to commence the gelling process of alginate and a solution of $CaCl_2$ being the crosslinker. The concentrations were optimized with 3 % (w/v) sodium alginate and 0.2 M $CaCl_2$. A liquid matrix of sodium alginate and recombinant subtilisin formed immediately upon mixing and was dropped in $CaCl_2$, it culminated in the development of a robust and stiff gel bead. The amalgamation of subtilisin inside the calcium-alginate bead yielded subtilisin activity of 170.5 U/mL and the maximum immobilization yield of 95.25 % was determined by equation (1).

3.2. Biochemical analysis of unbound and immobilized recombinant subtilisin

3.2.1. Influence of the pH level and temperature affecting the activity as well as durability of immobilized subtilisin

The major biochemical factors-pH and temperature are consistently recognized as crucial factors for assessing the optimal activity of proteins. According to previously reported, the engineered subtilisin demonstrated significant activity in the alkaline pH within the interval of 9–11, maintaining more than 90 % of its relative effectiveness, while reaching its peak efficiency at pH 10. When the recombinant subtilisin was immobilized with calcium alginate to form beads, it was subjected to pH assessment and stability check. The immobilized subtilisin was tested for the pH range of 3–13 which showed greater relative activity on the alkaline side (8–12) having >80 % as shown in Fig. 1A. The optimal level of pH was found out to be at pH 10 similar to free subtilisin

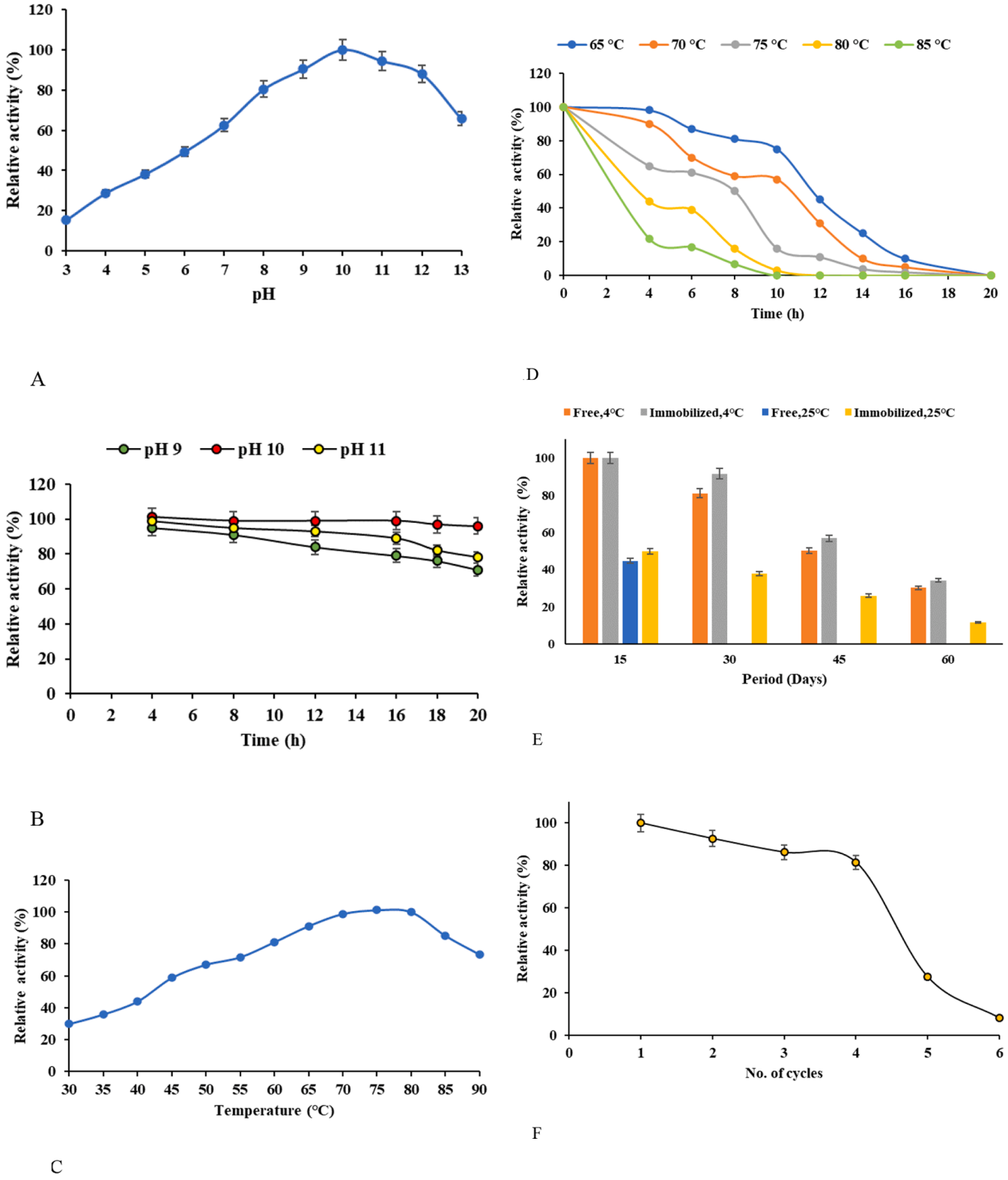

Fig. 1. Sodium alginate immobilization characterization- (A) Impact of pH (B) pH stability (C) Impact of temperature (D) Temperature stability (E) Storage (F) Reusability.

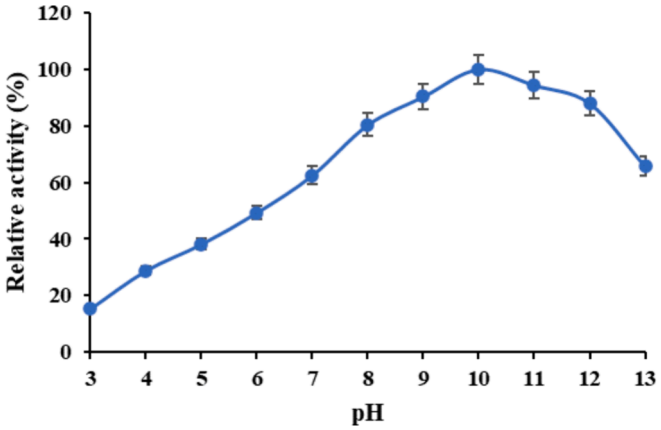

Fig. 1. (*continued*).

with slightly higher relative activity of 100 %. In the pH range of 3–5, less than 50 % of relative effectiveness had been noted for immobilized subtilisin. The reduction in performance in acidic circumstances might stem from alterations affecting the ionic states that surround the enzyme's sites of activity, which alter the molecular structure and folding characteristics of proteins. Nevertheless, in the elevated alkaline pH spectra spanning from 11 to 13, the relative activities were established in the range of 65 % to 94 %. No alteration in pH was detected upon entrapping the protein. Nevertheless, over a broad pH range, the entrapped subtilisin exhibited significantly enhanced enzymatic activity in comparison to soluble protein (Sattar et al., 2018). The stability of immobilized subtilisin under different pH conditions was examined through a 20-hour pre-incubation at pH 9, 10 and 11 at 35 °C. Immobilized subtilisin displayed notable resilience at pH 10 throughout the entire 20-hour period, maintaining over 96 % of its relative activity. Whereas at pH level 9 and pH level 11, the immobilized protein was stable up to 14 and 16 h respectively, with relative activities >71 % and >78 % respectively. As free subtilisin showed stability at pH 10 up to 20 h, immobilized subtilisin showed stability at pH range of 9–11 with 14–20 h of stability retained. This demonstrates the fact that this immobilized protein exhibits greater pH levels of activity and stabilization in the alkaline pH zone compared to the unbound subtilisin. This depicts the alkaline properties of the protein in Fig. 1B.

The immobilized subtilisin maintained its activity even at temperatures as high as 90 °C, exhibiting 88 % relative activity as evidenced in Fig. 1C. The immobilized protein was classified as an alkali-thermostable, with its optimal temperature determined to be 75–80 °C at pH 10. As purified recombinant subtilisin (free) had shown optimum temperature at 70 °C previously reported by Shettar et al., (2023b), the immobilized form has shown better relative activities and at higher optimum temperatures. The ability of subtilisin to withstand heat has been quantified within the temperature span of 65–85 °C for a duration of 2–20 h (Fig. 1D). The durations for which immobilized subtilisin maintained half of its activity at 65, 70, 75, 80, and 85 °C were recorded as 10, 10, 8, 6, and 6, respectively. As a result, the carrier calcium alginate was discovered to confer greater stability to subtilisin action, resisting the heat-induced agitation of subtilisin molecules induced through elevated temperatures.

3.2.2. *Storage and operational stability of the immobilized beads*

The enzyme/protein's shelf life dictates how long it can maintain its efficacy in a bioprocess. In general, the enzyme's active site degrades as it is stored in a liquid form for an extended time period. Enzymes are commonly stored in solutions, and the selection of storage conditions can significantly affect their shelf life. Temperature, pH, and the presence of stabilizing agents or cryoprotectants are important considerations. Regularly assessing enzyme activity over time is vital to ensure its continued effectiveness for the intended purpose. The storage durability of both soluble and subtilisin encapsulated in calcium alginate was examined at two temperatures of 4 and 25 °C for a span of 60 d and the relative activity was calculated every 15 d. At a temperature of 4 °C, it was discovered that the immobilized protein demonstrated superior stability, retaining 91.61 % of its original performance over 30 days, in comparison to the unbound protein, that preserved 81.01 % activity (Fig. 1E). Whereas, the immobilized subtilisin had 34.19 % relative activity up to 60 d of storage, while the free subtilisin showed 30.17 %. During a 60-day storage period at 25 °C, the soluble protein experienced nearly complete inactivation post 15 d. In contrast, the immobilized subtilisin retained 37.66 % of its original function under the same conditions at 30 d and 11.69 % upto 60 d of storage. The enhanced storage stability could be attributed to a decrease in enzyme denaturation or improved structural stabilization resulting from enzyme immobilization.

The capacity for repeated use of immobilized proteins is a critical aspect that significantly influences their economically efficient performance. This characteristic plays a pivotal role in minimizing costs associated with protein usage. Throughout the reutilization process, variations in the pH and temperature of the reaction system can impact both the durability of the carrier and the protein, potentially resulting in protein leakage and a subsequent decline in enzyme activity. As depicted in Fig. 1F, the protein immobilized exhibited sustained high reusability, with the relative activity consistently exceeding 81.52 % even after 4 cycles of reuse. This underscores the remarkable effectiveness of the immobilized enzyme in terms of reuse. Following the fourth cycle, the recorded relative activities stood at 27.57 % and 8.21 %, respectively. The progressive decline in relative enzymatic activities, particularly noticeable post the fourth cycle, might stem from the impact of repetitive centrifugation and washing forces, obstruction within the protein's catalytic site attributable to either the accumulation of compounds from oxidation on its exterior or otherwise the onset of leaky phenomena.

3.2.3. *Influence of various surfactants, metal ions, additives and organic solvents on free and immobilized subtilisin*

Treating recombinant and immobilized subtilisin with surfactants namely Tween 80, Tween 40, hydrogen peroxide and Triton X-100, as well as the ionic detergent SDS, yielded varying effects on relative enzymatic activity, as indicated in Table 1. The free protein retained maximum activity of 97.59 % and 95.97 % when subjected to 1 % SDS and Triton X-100 treatment. In terms of stability, it maintained 93.57 %, 90.44 % and 85.58 % activity when treated with 1 % Tween 80, Hydrogen peroxide and Tween 40. Researchers have illustrated that the aforementioned protein may withstand and reveal proteolytic functions under the influence of surfactants with names like Tween 40 and Triton

Table 1
Biochemical characterization of purified recombinant subtilisin and sodium alginate immobilized subtilisin gel bead- Impact of surfactants, metal ions, organic solvents, additives and substrate specificity.

Factors		Relative subtilisin activity (%)	
		Free subtilisin[a]	Immobilized subtilisin
Control	Without treatment	100	100
Surfactants	SDS	97.59 ± 0.3	85.04 ± 0.5
	Tween 80	93.57 ± 0.7	94.42 ± 0.7
	Triton X-100	95.97 ± 0.8	82.11 ± 0.1
	Tween 40	85.58 ± 0.6	92.66 ± 0.9
	Hydrogen peroxide	90.44 ± 0.3	80.93 ± 0.2
Metal ions	$FeSO_4$	67.03 ± 0.1	76.24 ± 0.3
	$MgSO_4$	94.07 ± 0.9	95.01 ± 0.4
	NaCl	86.75 ± 0.4	91.49 ± 0.9
	KCl	84.24 ± 0.7	83.87 ± 0.11
	$CaCl_2$	87.09 ± 1.1	89.74 ± 0.5
	$ZnSO_4$	98.10 ± 1.0	99.12 ± 1.1
	$CuSO_4$	101.22 ± 0.1	93.841 ± 0.5
Additives	PMSF	55.86 ± 0.7	62.17 ± 0.9
	dithiothreitol	90.78 ± 0.5	92.08 ± 0.7
	β-mercaptoethanol	89.32 ± 0.4	90.32 ± 0.5
	EDTA	95.58 ± 0.2	96.77 ± 0.8
Organic solvents	methanol	95.25 ± 1.1	97.95 ± 0.5
	ethanol	92.12 ± 1.0	87.98 ± 0.1
	ethyl acetate	94.80 ± 0.7	95.01 ± 1.0
	benzene	90.05 ± 0.8	89.74 ± 1.1
	glycerol	87.87 ± 0.3	88.56 ± 0.2
	chloroform	83.18 ± 0.5	84.46 ± 0.4
Substrate specificity	Casein		101.47 ± 0.5
	Azo-casein		99.71 ± 0.9
	ATEE		97.95 ± 1.0
	BTEE		99.12 ± 0.2
	N-Suc-F-A-A-F-*p*NA		101.76 ± 0.9

The relative activity lacking any surfactants, metal ions, inhibitors, or organic solvents was adopted as the control.
The data values reveal mean ± standard deviation.
The impact of 1 % surfactants, 0.5 M metal ions, 1 M additives and 10 % organic solvents were investigated for 30 min.
[a] Substrate specificity for free subtilisin has been previously published (Shettar et al., 2023b).

X-100, as well as surfactants like SDS at concentrations of 1 %. Consequently, this protein holds promise for various commercial applications, including detergent production. Among the lab detergents, immobilized subtilisin has shown the highest activity for Tween 80 followed by Tween 40 at 94.42 % and 92.66 % respectively. While it has also shown good stability for ionic detergent SDS and non-ionic Triton X-100 of 85.04 % and 92.66 % respectively. Tweens are non-ionic surfactants known for their ability to affect the fluidity and permeability of cellular membranes. Both Tween 40 and 80 have enhanced the relative activity in case of immobilized gel beads.

The consequence of numerous ions on the functioning of soluble versus immobilized subtilisin was examined. The current findings indicate that $MgSO_4$, $ZnSO_4$ and $CuSO_4$ enhance enzyme activity (93–101 %) in both free and immobilized subtilisin, serving as protective agents against denaturation as depicted in Table 1. However, KCl, NaCl and $CaCl_2$ does exert slightly lesser effects on the relative enzyme activity. In accordance with the aforementioned results, it is observed that $CuSO_4$ and $ZnSO_4$ enhances the effectiveness of both unbound and gel encapsulated protease, respectively and there is increase in the activity of immobilized recombinant subtilisin in case of $ZnSO_4$ (99.12 %) which goes in line with the other literatures reported (Nelson Ademakinwa et al., 2021; Thakrar and Singh, 2019). The elevated activity in an abundance of metals is most likely attributable to an extremophilic hydrothermal vent spot, wherein the atmosphere has been enhanced in heavy metals relative to the surrounding atmospheric environment.

Several additives were tested to assess the relative activities of free and immobilized recombinant subtilisin. Inhibitors are particular to proteins and can be employed for the taxonomy of proteins and work on activity. In the context of additives and inhibiting agents, the assessment of effectiveness was explored and outlined in Table 1. Studies on inhibition can offer valuable insights into the characteristics of a protein, its need for cofactors, and the characteristics of the active center. PMSF significantly inhibited both free as well as immobilized subtilisin (55.86 % and 62.17 %, respectively), even at a concentration as low as 1 M. Given that subtilisin is categorized as a serine protease, its activity was expected to be hindered in the company of PMSF, a phenomenon indeed observed in our study. PMSF has the capability to obstruct the serine residue within the enzyme's catalytic site, progressively as a consequence, there will likely be less activity (Farhadian et al., 2015). This suggests that the protein in question corresponds to the group of subtilisin-like serine protease category. The activity of effectiveness of unbound and gel encapsulated subtilisin remained unchanged in spite of the inclusion of EDTA, indicating that this protein is not reliant on metal ions or does not require divalent cations to sustain its activity. The immobilized gel bead has shown maximum relative activity of 96.77 % when compared to the unbound (free) enzyme, depicting that the immobilization using calcium alginate has indeed enhanced the effectiveness of the protein towards metals. The notable activity observed in the abundance of EDTA holds significant importance for potential applications in detergent formulation. This is particularly crucial as chelating agents like EDTA are commonly incorporated into detergents for their role as water softeners and stain removers (Gulmez et al., 2018).

The impact of organic solvents on protein stability exhibited a nearly uniform pattern. Methanol emerged as the most stabilizing solvent, affording a peak stability of 95.25 % for recombinant subtilisin, trailed by ethyl acetate, ethanol and benzene, all imparting a stability of 90.05–94.80 %. The least stability, at 83.18 %, was noted with chloroform (Table 1). The results suggest a substantial increase in recombinant subtilisin activity post-immobilization with calcium alginate, with improvements observed in various agents: methanol (97.95 %), ethanol (87.98 %), ethyl acetate (95.01 %), benzene (89.74 %), glycerol (88.56 %) and chloroform (84.46 %) as displayed in Table 1. Under the influence of organic solvents, enzymes can undergo inactivation and instability depending on the concentration. However, recombinant subtilisin retained its activity with the existence of certain organic solvents examined in this study. In a similar study, the protease named tamarillin from tamarillo fruit maintained approximately 96 % of its unprecedented activity in the abundance of ethanol, while retaining activity levels of up to 89 % and 85 % in methanol and glycol, respectively. The least activity retained was at 62 % when treated with chloroform. The enzymatic activity in the company of organic solvents could have been influenced by a multitude of factors. Disruption of hydrogen bonding, interactions with hydrophobic moieties, and modifications in protein charges may transpire, thereby impacting the dynamics and conformation of proteases, ultimately causing shifts in their catalytic processes (Li et al., 2018).

Table 2
Kinetics of Calcium alginate immobilized subtilisin.

Substrate	K_m (mM)[a]	V_{max} (X10^3 U/mg)[a]	k_{cat} (X10^3 min^{-1})	k_{cat}/K_m (X10^3 min^{-1} mM^{-1})
Casein	0.303 ± 0.5	19.095 ± 41	38.19	126.039
N-Suc-F-A-A-F-*p*NA	0.19 ± 0.3	10.7 ± 15	21.4	112.631

[a] The offered values are the average ± standard deviation of three separate batches enzyme evaluation.

3.2.4. Determination of substrate specificity of immobilized recombinant subtilisin

Empirical evidence from earlier studies verifies the discovery of recombinant subtilisin, demonstrating its selectivity in targeting hydrophobic in nature bases, including N-Suc-F-A-A-F-*p*NA, whereby aromatic residues of amino acids are located among the P1 and P4 locations (Shettar et al., 2023b). Following the activity measurements conducted with 20 g/L casein, 30 g/L azocasein, 10 mM ATEE and BTEE and 5 mM N-Suc-F-A-A-F-*p*NA aimed at elucidating the immobilized recombinant subtilisin protein's specificity toward different substrates, it was established that the protein exhibited its maximum activity in the presence of casein and N-Suc-F-A-A-F-*p*NA at 101.47 ± 0.5 and 101.76 ± 0.9 respectively (Table 1). It was also disclosed that the immobilized protein has demonstrated esterase and amidase activities by hydrolyzing ethyl esters in ATEE and BTEE. The presence of aromatic amino acids serves as a catalyst for robust activity at the catalytic site of recombinant subtilisin. Subtilisin can catalyze the dehydration of biologically and chemically modified proteins, and it also breaks down synthetic compounds. The substrate that determines the specificity of subtilisin relies on the precise amino acids earlier than the bond between peptides targeted for cleavage.

3.2.5. Kinetic studies of immobilized subtilisin

The Lineweaver-Burk graph was implemented for examining the kinematic features of the immobilized subtilisin, and its findings have been displayed in Table 2. Immobilized subtilisin demonstrated the classic kinetics of Michaelis–Menten. The enzymatic activity progressively rose with a boost in substrate concentration, eventually reaching the point of saturation, indicating an exhaustion of the enzyme's active sites. V_{max} denotes the peak rate attained when enzyme is completely swamped with substrate concentration. The Michaelis constant (K_m), referring to the quantity of substrate for which the rate of response approaches halfway of its maximal rate (V_{max}), serves to measure the substrate hydrolysis affinity of the immobilized subtilisin. The K_m points for the casein and synthetic peptide as substrates had been determined to be 0.303 ± 0.5 and 0.19 ± 0.3 mM, correspondingly, while the V_{max} attributes were 19.095 ± 41 × 10^3 and 10.7 ± 15 × 10^3 U/mg, correspondingly. A lowering K_m value indicates improved specificity for the substrate and a high affinity for adhering to it. The K_m values indicate the fact that the N-Suc-F-A-A-F-*p*NA has a higher affinity for immobilized subtilisin. The calculated k_{cat} for casein was 38.19 × 10^3 min^{-1}, with a deduced catalytic efficiency (k_{cat}/K_m) of 126.039 × 10^3 min^{-1} mM^{-1}. For N-Suc-F-A-A-F-*p*NA, the calculated k_{cat} was 21.4 × 10^3 min^{-1}, and the deduced catalytic efficiency (k_{cat}/K_m) was 112.631 × 10^3 min^{-1} mM^{-1}. In a compelling previous investigation involving purified recombinant subtilisin, a decrease in the K_m for the specific substrate was noted, suggesting an enhanced specificity of the serine protease towards the substrate. Additionally, the recombinant subtilisin exhibited heightened specific activity and catalytic efficiency (Shettar et al., 2023b). The enhanced K_m and V_{max} measurements of the immobilized subtilisin when contrasted to the previous work demonstrate that the immobilization of the protein inside a calcium alginate gel bead has boosted its efficiency for the substrates examined.

3.3. Nanoparticles made of silver and zinc oxide linked with recombinant subtilisin: Synthesis and characterization

The key proof for the efficient combination of previously investigated recombinant subtilisin coming from *B. subtilis* combined with multiple silver nitrate compositions (5, 10 and 50 mM each) experienced the obvious change that occurred in the concoction's shade, transitioning from pastel yellow towards a deep brown hue. This was

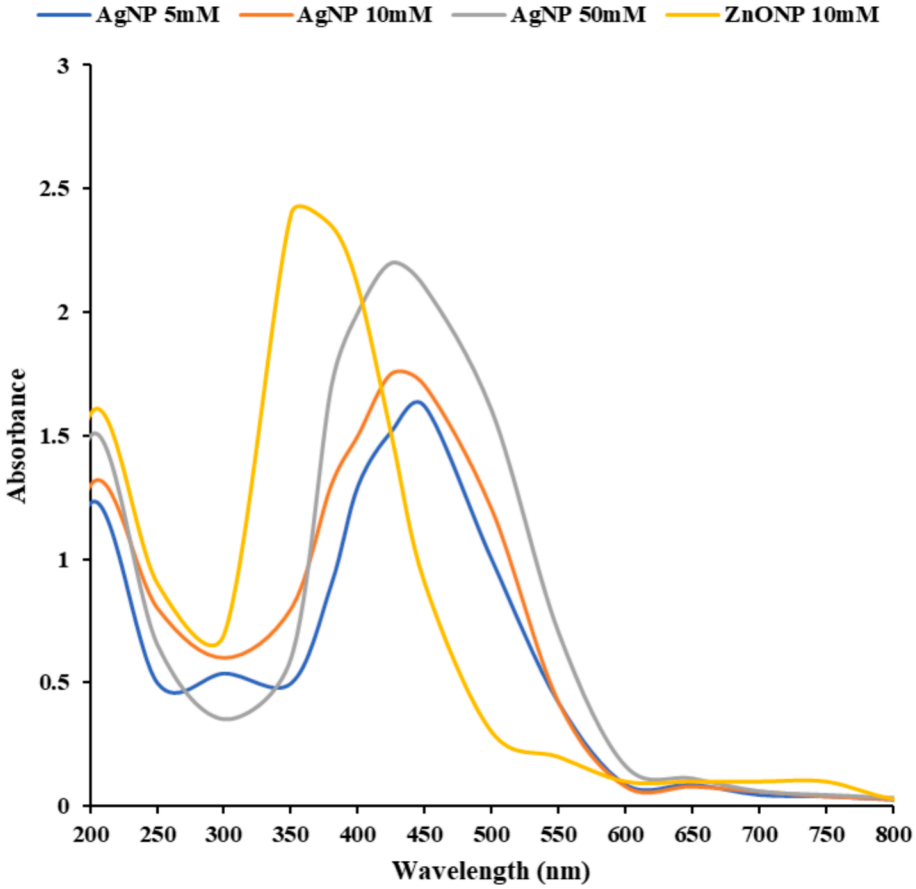

Fig. 2. UV–Visible spectroscopy of recombinant subtilisin capped nanoparticles.

confirmed after gestation, and the combined mixture effectively streamlined the transformation of aqueous ions of silver (Ag^{+}) into silver nanoparticles (AgNP) via reduction. The discernible alterations to heterogenous mixture tint provided as a preliminary sign of the biosynthesis of recombinant subtilisin-capped silver nanomaterials (Sidhu and Nehra, 2020). The availability and volume of silver nanoparticles (AgNP) were verified using a spectrophotometer with ultraviolet (UV) radiation. Under UV illumination, the measured peaks at a wavelength of 450 nm for 5 mM dosage and a wavelength of 425 nm for 10 mM and 50 mM corroborated the existence of AgNP. The existence of AgNP has been proven since their characteristic scale typically ranges around 400–470 nm. Fig. 2 depicts the wavelength absorption patterns plotted. The presence of unbound electrons in nanoparticles promotes the formation of an electromagnetic surface plasmon resonance (SPR) wave. This band is caused by the coordinated oscillations of free electrons in AgNP, which resonate with the fluctuating electric field of the incoming light.

The initiation of zinc oxide nanoparticles (ZnONP) formation took place as 700 µL of a 10 mM zinc acetate solution was incorporated gradually drop by drop into 300 µL of the recombinant subtilisin, all while stirring and incubating at 55 °C. The reaction mixture transitioned from its original color to a yellowish hue and eventually to a cream-colored precipitate. The appearance of Surface Plasmon Resonance (SPR) was associated to this modification in ZnONP, serving as an indication of the formation of nanoparticles. The ultraviolet–visible approach was applied in order to track the process of synthesis of nanoparticles made up of zinc oxide and the concomitant reduction from Zn^{2+} to ZnONP. Mei's hypothesis contends, the generated nanomaterial with just one point of absorption in the UV spectrum is more probable to possess a shape that is spherical. A prominent spike located in the UV zone spanning 300–400 nm in wavelength denotes an abundance of nanoparticles of zinc oxide. In this study, significant peak at 350 nm was discerned, providing evidence for the manufacturing of ZnONP in the amalgamation with recombinant subtilisin.

3.4. Functional characterization of recombinant subtilisin capped nanoparticles

3.4.1. Evaluation of antibacterial activity (AMA) and minimum inhibitory concentration (MIC)

The discovery of alternative antimicrobial medications is critical in tackling the evolving issue of antibiotic resistance. Naturally accomplished products, extracts from plants, and nanoparticles with inhibitory effects on organisms serve as essential elements in the fabrication of inexpensive antimicrobial solutions. In the course of currently underway investigation, the antibacterial activity and MIC in pure recombinant subtilisin bound nanoparticles (Ag and ZnO) have been investigated against both Gram-negative as well as positive test organisms. The antimicrobial effectiveness of the encapsulated nanoparticles created by the process of biosynthesis has been demonstrated to be powerful against all test species described in this study. The experiment was replicated on three occasions, and the findings were interpreted based on the average diameter of the inhibition zone. As summarised in previous study reported by Shettar et al., (2023b), it elucidates that recombinant subtilisin exhibited the highest clearance zone (mm) against Gram-positive bacteria such as *B. licheniformis* (30.1 ± 0.2 mm) and *B. cereus* (26.4 ± 0.5 mm), surpassing *S. aureus* (18.2 ± 0.3 mm) and *E. coli* (19.3 ± 1.1 mm), *P. aeruginosa* (18.5 ± 0.6 mm) and *S. typhimurium* (18.3 ± 0.7 mm) for Gram-negative bacteria. The current examination displays that the recombinant subtilisin was conjugated with AgNP and ZnONP and assessed for its antibacterial activities against different test organisms. Noteworthy effectiveness was demonstrated by recombinant subtilisin bound AgNP and ZnONP 50 mM each, with the latter displaying substantial inhibition against *B. licheniformis* (36.9 ± 0.4 mm) and *E. coli* (26.5 ± 0.7 mm) respectively, as shown in Table 3. *S. aureus* exhibited a marginally lower inhibitory effect for the capped nanoparticles. The noted inhibition of test organisms' growth suggests that silver ions were emitted by the metallic nanoparticles. In terms of antibacterial efficacy, subtilisin-capped nanoparticles not only illustrated improved antibacterial capacity but also demonstrated a more extensive spectrum of antibacterial response when juxtaposed with subtilisin alone. Cefixime, the positive control, indicated inhibitory zones that varied between 14.5 ± 0.8 and 26.4 ± 0.3 mm, as displayed in Table 3.

Subsequent to this, Minimum Inhibitory Concentration (MIC) analysis was conducted to assess bacterial development in the abundance of progressively diluted capped nanoparticles. The findings were reviewed visually as well as by documenting the growth trend at 600 nm. The MIC of recombinant subtilisin was studied and reported earlier within the range of 0.06–0.9 µg/mL (Shettar et al., 2023b). Table 4 summarizes the effectiveness of the current investigation's bound AgNP and ZnONP against the two Gram-positive along with negative test organisms. Following CLSI recommendations, the MIC was established employing the conventional microbroth dilution approach. The MIC analysis revealed that subtilisin bound zinc oxide nanoparticles (ZnONP) demonstrated the lowest values for *B. cereus* and *B. licheniformis* at 0.097 mM, with *P. aeruginosa* and *S. typhimurium* following closely at 0.195 mM. *S. typhimurium* showed the highest MIC value, recorded at 0.9 µg/mL for recombinant subtilisin studied previously. AgNP has a comparable inhibitory concentration against *B. licheniformis* alone. This study identified that recombinant subtilisin-conjugated nanoparticles (AgNP and ZnONP) had superior antibacterial efficacy than recombinant subtilisin individually.

3.4.2. Assessment of antioxidant activity

3.4.2.1. DPPH scavenging activity. Antioxidants in nanoparticles perform an indispensable function in shielding the building blocks of tissues and cells against damage from oxidation induced by oxygen molecules called reactive oxygen species (ROS). Incorporating antioxidants into nanoparticles amplifies their effectiveness in diverse sectors and fields within biomedicine, making a substantial contribution to across-the-board health improvement. In this current investigation, the antioxidant potential of recombinant subtilisin bound nanoparticles made of Ag and ZnO were examined employing DPPH and ABTS radical

Table 3
Antibacterial activities of recombinant subtilisin synthesized nanoparticles against test organisms.

AMA		Gram positive test organisms			Gram negative test organisms		
		Bacillus cereus	*Staphylococcus aureus*	*Bacillus licheniformis*	*Pseudomonas aeruginosa*	*Escherichia coli*	*Salmonella typhimurium*
Inhibition zone diameter (mm ± SD)	AgNP 10 mM	24.1 ± 0.4	16.2 ± 0.7	27.6 ± 0.6	17.1 ± 0.9	15.1 ± 0.5	17.9 ± 0.9
	AgNP 50 mM	31.5 ± 0.8	23.9 ± 0.8	33.4 ± 0.7	20 ± 0.1	20.9 ± 0.5	21 ± 0.1
	ZnONP 10 mM	24.6 ± 0.6	13.2 ± 0.5	25.3 ± 1.2	16.5 ± 0.5	18.4 ± 0.1	20.5 ± 1.0
	ZnONP 50 mM	35.7 ± 0.3	24.1 ± 0.5	36.9 ± 0.4	25.2 ± 0.6	26.5 ± 0.7	25.1 ± 0.3
	Cefixime	22.3 ± 0.5	14.5 ± 0.8	26.4 ± 0.3	16.8 ± 0.7	20.1 ± 0.2	14.8 ± 0.5

Table 4
MIC of recombinant subtilisin bound nanoparticles- made of Ag and ZnO.

MIC		Gram positive test organisms			Gram negative test organisms		
		Bacillus cereus	*Staphylococcus aureus*	*Bacillus licheniformis*	*Pseudomonas aeruginosa*	*Escherichia coli*	*Salmonella typhimurium*
MIC (mM)	AgNP	0.195	0.39	0.097	0.39	0.195	0.39
	ZnONP	0.097	0.39	0.097	0.195	0.39	0.195

Table 5
DPPH radical scavenging activity of recombinant subtilisin capped Ag and ZnO nanoparticles.

Silver nanoparticle	Zinc oxide nanoparticle		Ascorbic acid	
Concentration (mM)	Scavenging activity (%)	Scavenging activity (%)	Concentration (μg/mL)	Scavenging activity (%)
5	38 ± 0.07	48 ± 1.0	10	66 ± 0.07
10	49 ± 0.05	51 ± 0.1	20	72 ± 0.02
20	57 ± 0.9	63 ± 0.9	30	79 ± 0.4
30	68 ± 0.06	74 ± 0.2	40	85 ± 1.2
40	76 ± 0.1	83 ± 0.05	50	88 ± 1.0
50	89 ± 0.01	92 ± 0.03	60	89 ± 0.9

The data values indicate the average ± standard deviation of three separate experiments and are statistically significant at $p < 0.05$.

scavenging approaches. The selected methodologies in this study were known for their simplicity, speed, sensitivity, and effectiveness in evaluating the scavenging activity of nanoparticles synthesized through biological processes. The DPPH test is significant because it may evaluate a substance's antioxidant or free radical-scavenging capabilities. The fundamental principle of the DPPH assay revolves around assessing the capacity of a substance to counteract the stable unbound radical DPPH (2,2-diphenyl-1-picrylhydrazyl). The observable shift in color, transitioning from purple to yellow, is directly correlated to the scavenging activity, offering a measurable indication of the substance's prowess in antioxidant function (Chojniak-Gronek et al., 2022). As previously reported, the scavenging activity for recombinant protein within the concentration range of 10–60 μg/mL, reaching its peak at 50 μg/mL with 86 % inhibition (Shettar et al., 2023b). As indicated in Table 5, the inhibition at 89 ± 0.9 %, was observed for ascorbic acid, serving as the reference standard. The highest scavenging activity, at 92 %, was noted for ZnONP at a concentration of 50 mM, followed by 89 % for AgNP at the same concentration even after 30 min of incubation.

3.4.2.2. ABTS scavenging activity. The blue chromophore ABTS•+ is generated through the chemical interaction amongst ABTS and potassium persulfate. In the presence of the protein or ascorbic acid, the ABTS•+ cation radical undergoes reduction. The concentration of the remaining radical cation after reacting with the antioxidant moiety is then quantified. Recombinant subtilisin has recorded maximum inhibition of 51 % at time 60 h as reported previously (Shettar et al., 2023b). In the present study, recombinant subtilisin conjugated AgNP and ZnONP have been examined. The highest scavenging activity against ABTS•+ radical cation was recorded at 97 % at time point of 60 h for recombinant subtilisin-capped ZnONP (Fig. 3A). This was compared with the standard butylated hydroxytoluene, showcasing its antioxidative activity at 46 %. At the identical concentration, AgNP exhibited a scavenging activity of 61 % at 60 h. A review of the research results depicts that, all sample quantities were pretty successful in scavenging free radicals that were present. Notably, ZnONP performed admirably in both antioxidant assays, indicating that it can serve as a promising antioxidant. The study's trials were all done in triplicates, and the average of all the independent batches was adopted to arrive at the ultimate results. This method ensured statistical dependability while mitigating the influence of any data fluctuation or outliers.

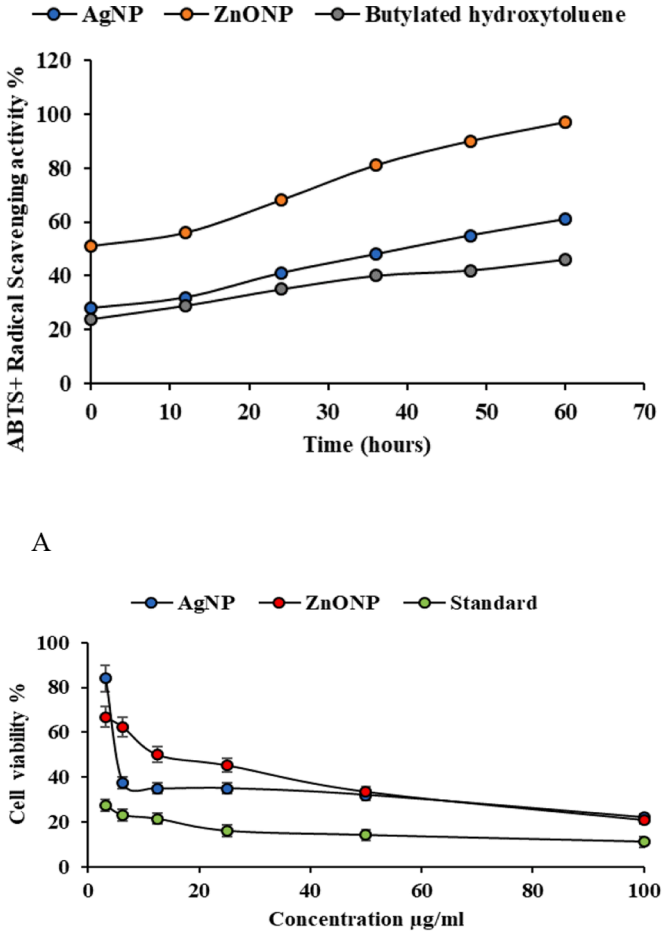

Fig. 3. Functional characterization of recombinant subtilisin-like serine protease capped nanoparticles. (A) Antioxidant activity by ABTS method (B) MTT assay of capped nanoparticles against cell lines of breast cancer.

3.4.3. Assessment of anticancer activity by MTT assay

The MTT test has been employed for investigating the cytotoxic impacts on various doses of recombinant subtilisin bound AgNP and ZnONP on breast cancer cells in humans MCF-7 cell types are a good method to measure cell development. Recombinant subtilisin was examined for its anticancer capability and revealed to be having a dose-dependent pattern on A549 as well as MCF-7 cell line as studied previously (Shettar et al., 2023b). *In vitro*, recombinant subtilisin-capped nanoparticles have been investigated for cytotoxicity against MCF-7 malignant cell lines at concentrations spanning from 3.125-100 μg/mL to determine cell viability. Cell viability reduced dose-dependently as the concentrations of AgNP and ZnONP rose. ZnONP demonstrated higher activity than AgNP as shown in Fig. 3B. The IC_{50} value for MCF-7 cell lines, representing the actual dose of recombinant protein needed to limit cell growth by 50 %, was determined. The results of the

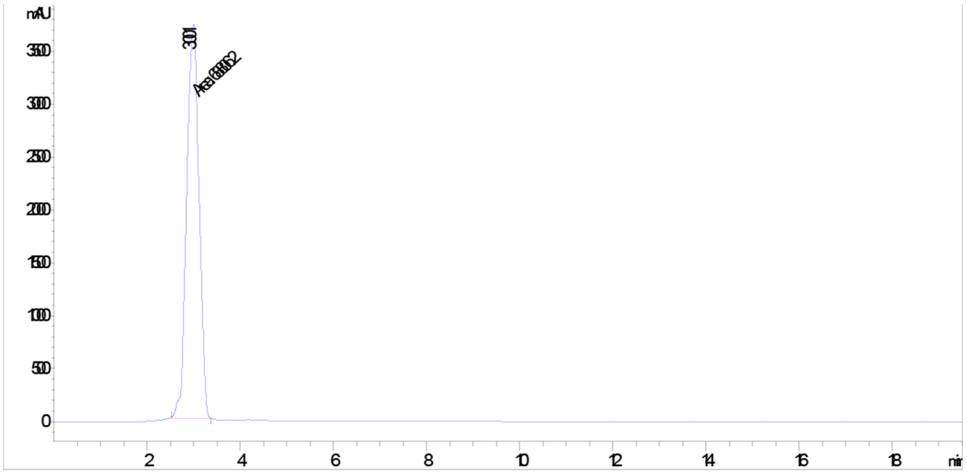

A

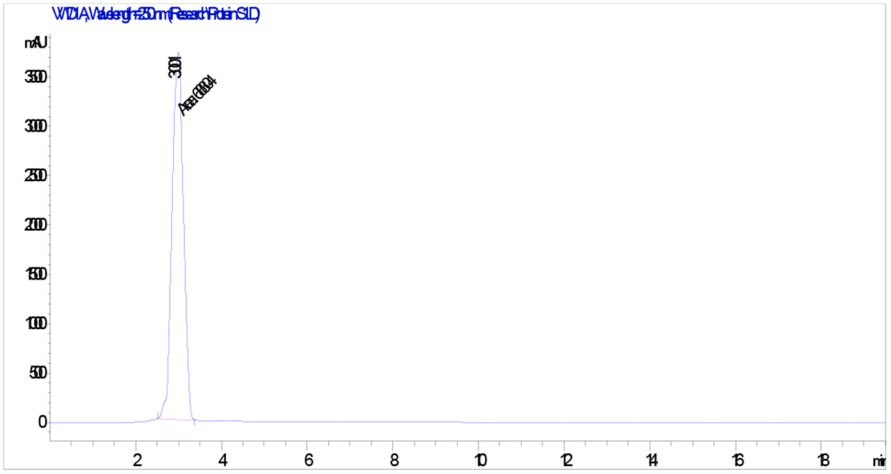

B

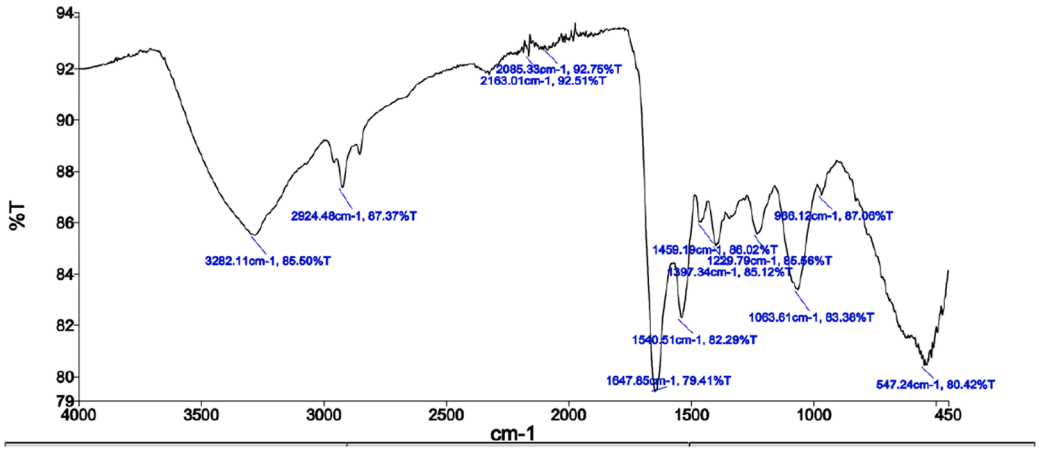

C

Fig. 4. Bioanalytical characterization of purified recombinant subtilisin and subtilisin capped nanoparticles. (A) HPLC analysis of purified recombinant subtilisin, (B) HPLC of standard surfactin (C) FTIR assessment of AgNP, (D) FTIR assessment of ZnONP, (E) SEM examination of AgNP, (F) EDS examination of AgNP, (G) SEM analysis of ZnONP, (H) EDS analysis of ZnONP, (I) TGA of AgNP (J) TGA of ZnONP, (K) AFM examination of AgNP, (L) AFM examination of ZnONP.

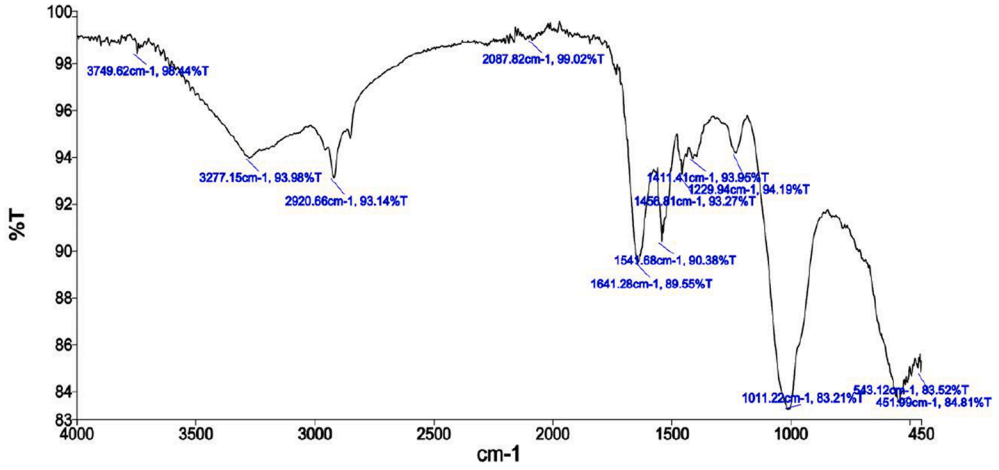

D

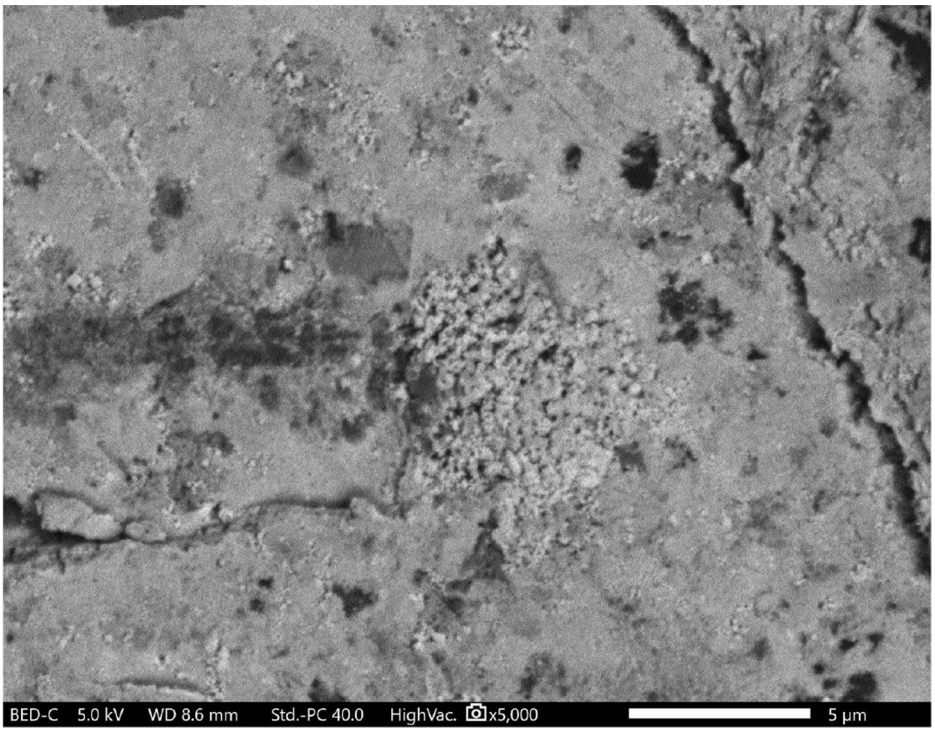

E

Fig. 4. (*continued*).

computation for AgNP as well as ZnONP were 8.87 µg/mL and 14.52 µg/mL, correspondingly. Doxorubicin, the control medication, has an IC_{50} of 3.62 µg/mL (Shettar et al., 2023a).

3.5. Analytical characterization of purified recombinant subtilisin and its capped nanoparticles

3.5.1. HPLC (High Performance Liquid Chromatography) analysis of recombinant subtilisin

The HPLC examination of the purified recombinant subtilisin revealed a major peak occurring at a retention time (RT) of 3.001 min with mobile phases methanol: water at the ratio of 70:30 and 0.5 mL/min flowrate. The detector with variable wavelength was set at 254 nm. This corresponds to the standard surfactin (Sigma-Aldrich) produced by *B. subtilis,* displaying a single peak at exactly the same retention time 3.001 min.

3.5.2. FTIR assessment of recombinant subtilisin capped nanoparticles

In the continuing work, FTIR analysis on recombinant subtilisin-capped Ag and ZnONP suggested that they were composed of distinct troups demonstrating behavioral characteristics. C-O (carbon–oxygen) as well as C-N (carbon–nitrogen) chains stretching among amides, OH,

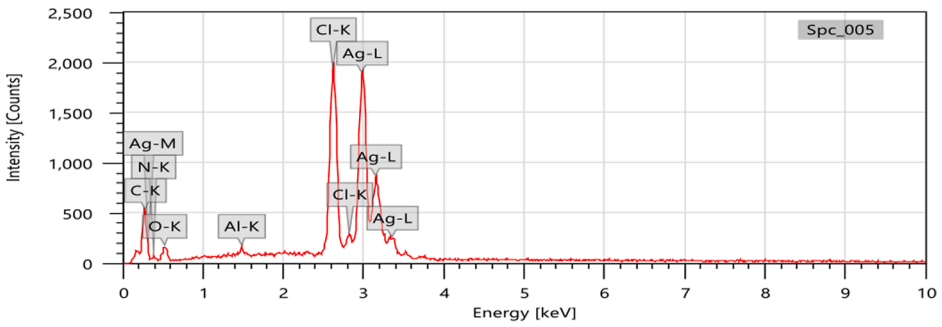

F

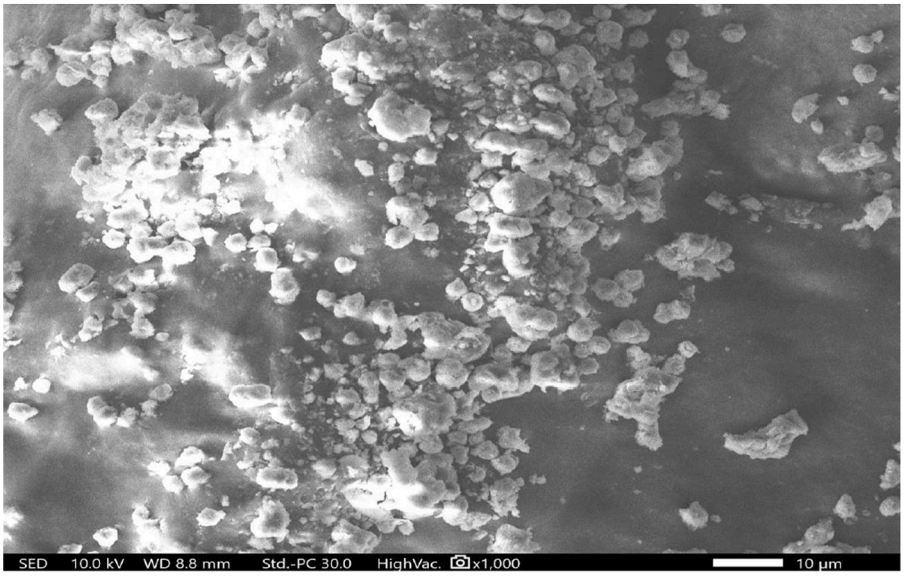

G

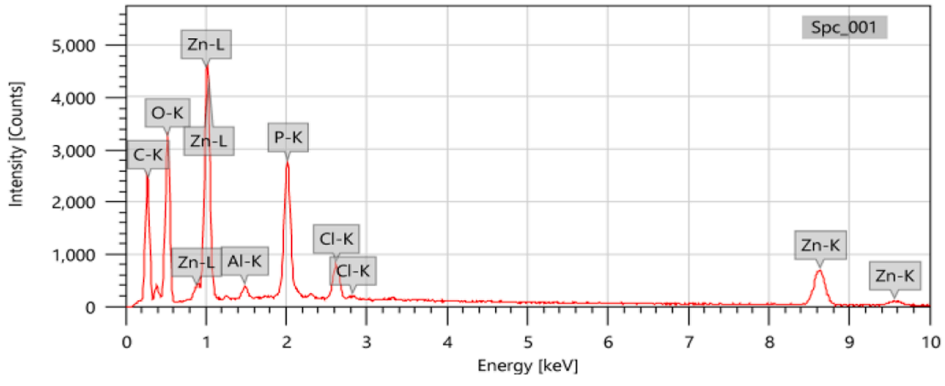

H

Fig. 4. (*continued*).

and NH_2 categories, in addition to C–H extending and the alkynes with C–C flexibility are included. Several significant bands in the FTIR spectrum were observed, each signifying the presence of distinct functional groups which are associated with both the nanoparticles, as illustrated in Fig. 4C and 4D. The apparent existence of amide bands, illustrated as a large peak of absorption at 3282 cm^{-1} (maxima), validates the N–H lengthening mode and the OH stretch of hydrogen bonds. The wavenumber of 2924 cm^{-1} vibrations associated with aliphatic (non-aromatic) carbon-hydrogen (C–H) bonds are detected in the infrared spectrum. The infrared spectrum typically shows typical

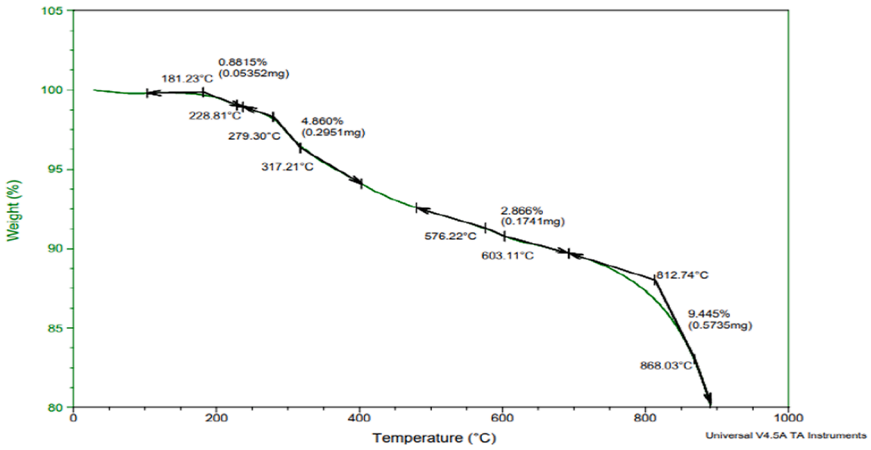

I

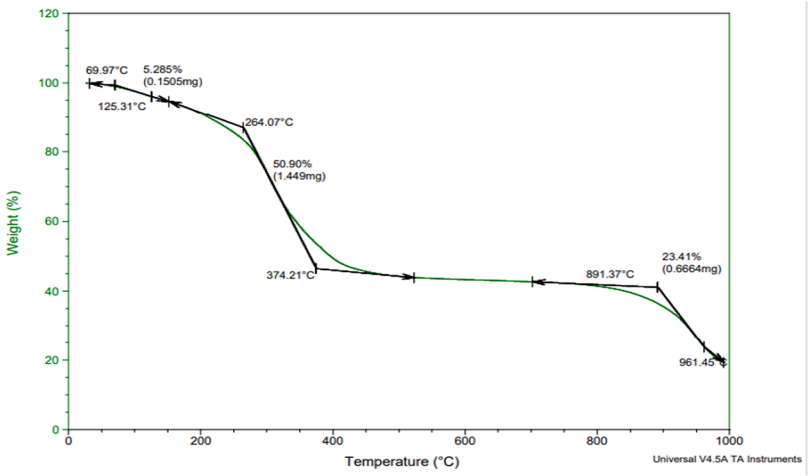

J

Fig. 4. (*continued*).

symmetric elongation of alkyne bridges (−C–C═C) about 1535–1580 cm^{-1}. The primary Amide II wave is located at 1540 cm^{-1}, whereas Amide III wave is centered at 1397 cm^{-1}. The amide I band is critical for structural investigation via FTIR imaging due to the fact that it provides significant data about the protein's secondary structures which include alpha-helical, beta-sheet, alongside randomized coils. It is usually found in the region between 1350–1750 cm^{-1}. The existence of amide groups, specifically −C-N and carbonyl groups (−C═O) that compose the vibratory stretching of peptides and protein molecules, is denoted by the strong signal detected at 1647 cm^{-1} (Sharma et al., 2018). Furthermore, a peak in absorption at 1459 cm^{-1} could have been attributed to the oscillation produced by the C–H alkyl bridge between aliphatic amino acid units namely leucine and isoleucine The major spike at 1063 cm^{-1} in the silver nanoparticle FTIR spectra corresponds to the –C–N stretching of aliphatic amines or phenolic/alcoholic compounds with an aliphatic structure. The prominent spike at 547 cm^{-1} has been attributed to vibrations involving Ag-O bonds. It refers to the association of ions made up of silver or silver particles with functional groups that include oxygen or biomolecules in the framework of nanoparticles or silver-containing materials.

Fig. 4D's absorption peaks give vital information regarding the molecular makeup and content of the biomolecules participating in the biosynthesis process, assisting in the characterization of zinc oxide nanoparticle (ZnONP) generation. The spike at 3277 cm^{-1} has been attributed to the –OH stretching of phenolic or alcoholic molecules with the –NH stretch of amines. The elongation peak of groups consisting of –OH appears to range between 3600 and 3200 cm^{-1}, affirming an existence of water molecules that are on the outermost layers of nanoparticles made of zinc oxide. The functional categories related to both the C-O and C–H stretching patterns are demonstrated by peak sizes ranging around 1500 to 1700 cm^{-1} and 2500 to 2900 cm^{-1}, respectively. The bend at 1641 cm^{-1} displays the C-O vibration as mentioned above and amide group –C–N (Fig. 4D). The extensive major peak at 1011 cm^{-1} reflects the frequencies of the functional categories such as C–C, C-OH, and C–H. The prominent peak at 451 cm^{-1} is attributable to Zn-O bending, indicating an existence of ZnO and the synthesis of ZnONP thereby resulting in the diminution of metal ions to metallic nanoparticles.

3.5.3. SEM with EDS assessment of recombinant subtilisin capped nanoparticles

SEM combined with EDS images offer additional insights into the morphology, chemical and size distribution of the recombinant subtilisin bound AgNP and ZnONPSEM photography can be employed to get

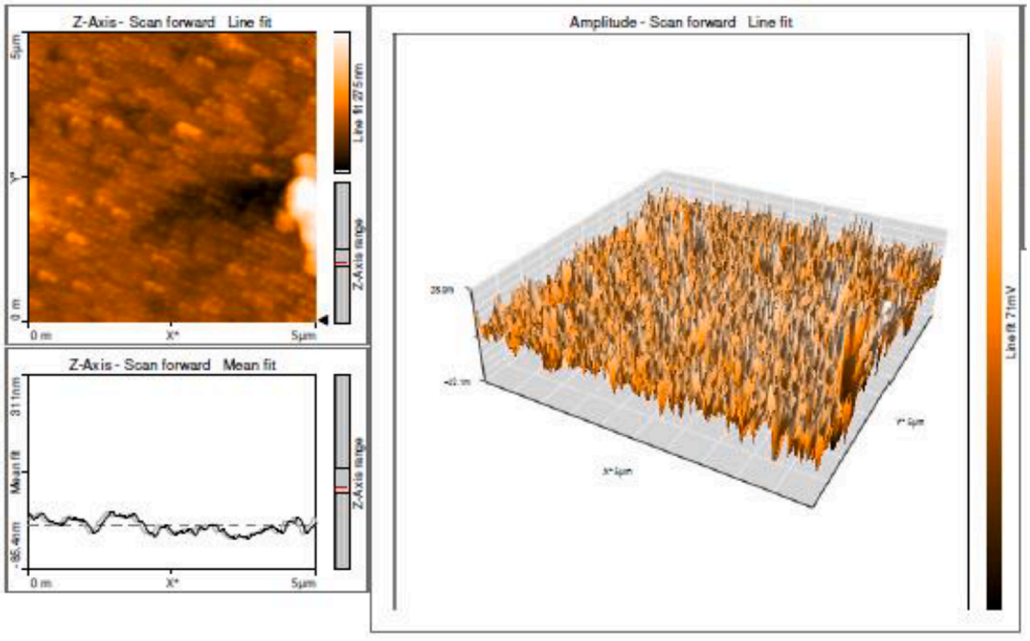

K

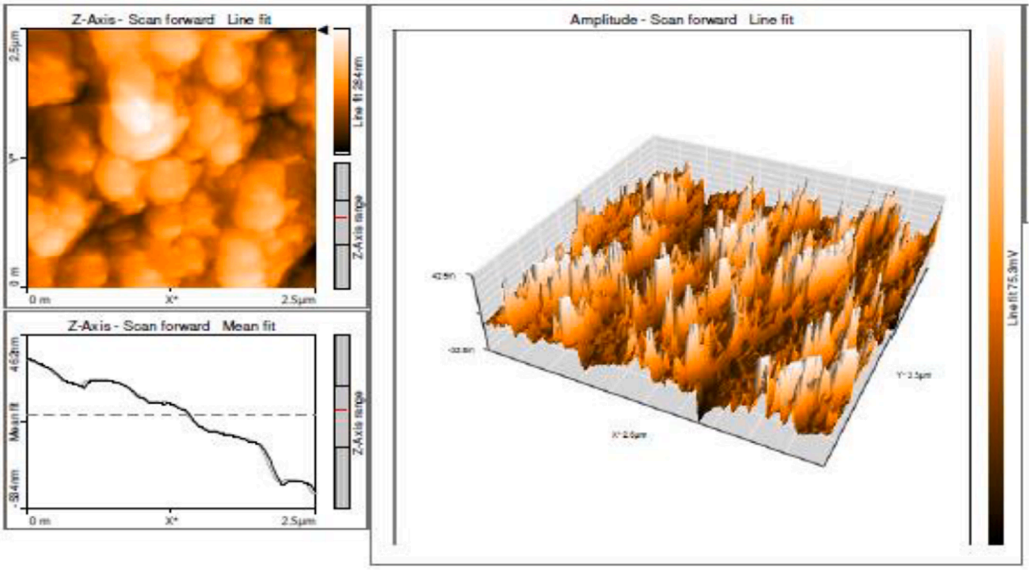

L

Fig. 4. (*continued*).

detailed photographs of a sample's surface anatomy. EDS analyzes element distribution by recognizing X-rays emitted via the product being investigated when struck by an electron laser. The SEM investigation was carried out on the dehydrated Ag nanoparticles. The clusters of nano-composites containing extremely small silver nanoparticles co-embedded with recombinant subtilisin is depicted in Fig. 4E. These formations exhibited a morphology resembling bacilli and curved structures. The accumulations could have arisen as a consequence of the process of dehydration. The detection of the silver element in the AgNP spectrum was established subsequently by the EDS study demonstrated in Fig. 4F. A more substantial spike around 3 keV (binding energies), demonstrating an abundance of particles of silver within the reduced state, confirmed the diminution of silver ions Ag^{+} to Ag^{0}. Pursuant to the spectra, silver was the most abundant portion, occupying 46.54 % of the whole, accompanied by carbon (23.03 %), chlorine (14.60 %), and impurities (15.82 %), representing the emergence of silver nanoparticle bound recombinant subtilisin (data not shown).

According to the observations from scanning electron microscopy (SEM), the involvement of recombinant subtilisin proved to be highly effective in the biosynthesis of nanoparticles made up of zinc oxide

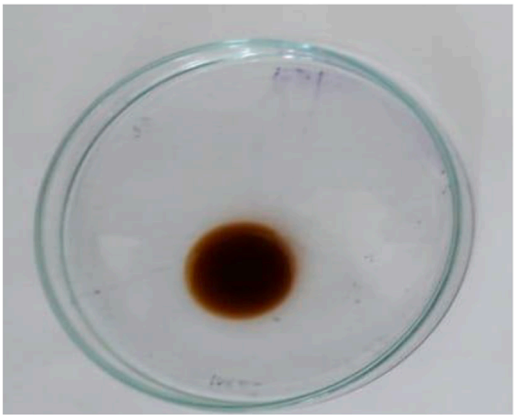

A

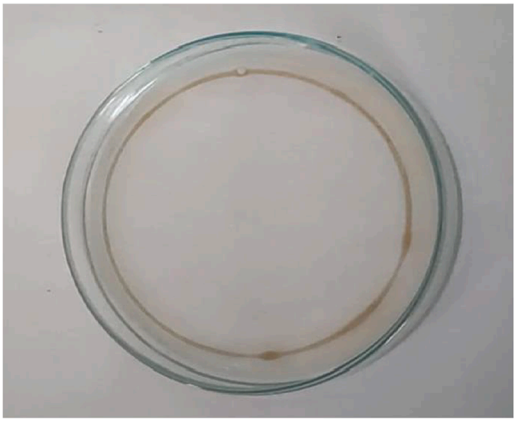

B

C

Fig. 5. Applications of pure recombinant subtilisin (A) biosurfactant activity of control, (B) biosurfactant activity of recombinant subtilisin (C) dehairing of goat hide with control, (D) dehairing of goat hide with recombinant subtilisin (E) blood stain removal-(a) Control, (b) detergent, (c) recombinant subtilisin, (d) detergent + recombinant subtilisin and (F) Dissolution of blood clot-(a)Control, (b) recombinant subtilisin.

D

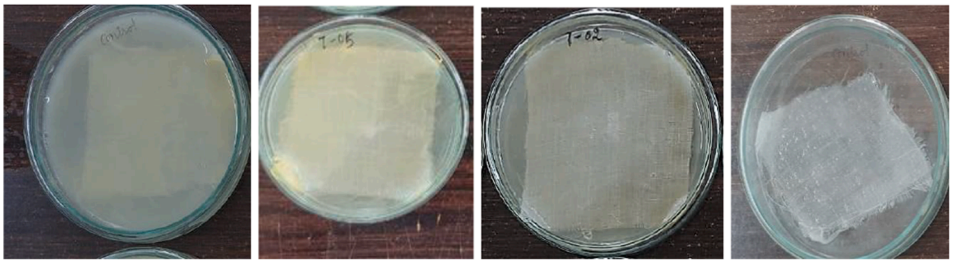

a b c d

E

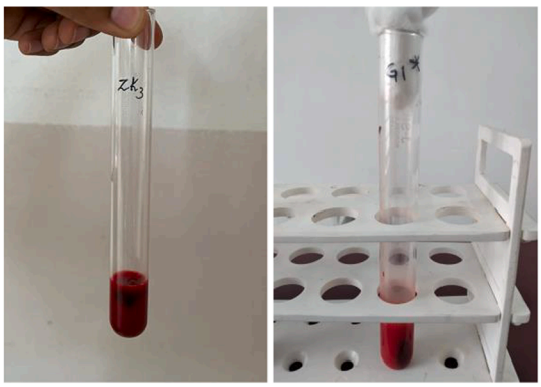

a b

F

Fig. 5. (*continued*).

(ZnONP). The findings indicated that recombinant subtilisin capped-ZnONP displayed a rounded structure, although not entirely smooth, with a reasonably even and consistent distribution and uneven texture (Fig. 4G). Energy-Dispersive X-ray Spectroscopy (EDS) results may be utilized for verifying ZnONP purity and composition. The data typically shows an individual signal for zinc (Zn) and oxygen (O) components, affirming that there is an amount of ZnO within the sample, with distinctive signals detected between 0.5–1 keV, 8.6 keV, and 9.6 keV,

respectively (Fig. 4H). As per the EDS spectra, the predominant element detected was zinc (Zn), constituting 17.54 %, followed by carbon at 38.21 %, along with other unidentified substances (data not shown). The sheer amount of carbon depicts that recombinant subtilisin participate in the diminution and coupling of bio-synthesized ZnONP.

3.5.4. TGA of recombinant subtilisin capped nanoparticles

TGA is a technique employed to study the differences in weight of a material as a matter of temperature. In the context of AgNP and ZnONP, TGA would involve subjecting the silver and zinc oxide nanoparticles to a controlled temperature increase while measuring the corresponding weight loss. This helps in understanding the thermal stability of the nanoparticles, as different materials exhibit varying degrees of weight loss at specific temperature ranges. The analysis provides essential knowledge on the decomposition, stability, and thermal behavior of the nanoparticles under heating conditions. The TGA investigation found multiple phases of dropping weight. In Fig. 4I, a modest fall of 0.88 % appeared during the beginning phase of weight loss (<200 °C), which was attributable to the dissipation of physiosorbed water from the surface remaining on the AgNP. Between 228 and 812 °C, the second stage of weight reduction, amounting to 4.860 % and 2.866 % respectively, takes place, involving the breakdown and evaporation of organic and bioactive compounds potentially existing on the sample being tested, namely surfactants, stabilizers, or capping agents. At temperatures exceeding 800 °C, the silver nanoparticles exhibit their core component disintegration while being capped. After a minor loss, the system stabilizes. The grade of the biosynthesized AgNP is assessed to be 81.92 % pure silver.

In case of recombinant subtilisin capped ZnONP, the preliminary phase of weight reduction, spanning from ambient temperature to 264 °C, indicated a minor decrease of 5.285 %, implying the elimination of water molecules situated on the nanoparticle surface (Fig. 4J). Post 264 °C and upto 374 °C, a substantial weight decrease of 50.90 % is observed, attributed to the degradation and abrupt evaporation of the sample. The lack of residues around 500–700 °C indicates that the structure of recombinant subtilisin-capped ZnONP underwent decomposition, producing gases and resulting in the formation of carbonaceous char. This temperature range likely led to the breakdown of organic components, leaving behind volatile products and carbon residues. At ~ 888 °C, the weight dropped by 23.41 %, indicating further disintegration and vaporization of residual chemicals that are bioactive. At this level of temperature, numerous biological molecules including impurities are predicted to be eliminated, leaving behind highly pure zinc oxide nanoparticles (Özbek and Ünal, 2017).

3.5.5. AFM of recombinant subtilisin capped nanoparticles

AFM allows researchers to acquire pictures with excellent resolution and altitude measurements via sweeping the tip of a pointed object across the topography of nanomaterials. When the point of the AFM strikes the sample surface, the cantilever bends owing to attraction and repulsion processes among the atoms and molecules that are upon the pointed end of the instrument as well as its external surface. The measurement entails recording the angle of deflection caused by the cantilever, and a system of feedback serves to establish a constant pulling force across its tip and the object being measured. As shown in Fig. 4K, the AFM visualization of AgNP illustrates the generation of aggregates with a sphere-like form and evenly spaced distribution. The biosynthesized recombinant subtilisin capped ZnONP's surface features were meticulously examined and visualized at the nanoscale through AFM, employing both 2D and 3D topography analysis. The AFM photographs displayed the external shape and ruggedness of zinc oxide nanoparticles capped with recombinant subtilisin in Fig. 4L. These findings imply indicate the pattern of distribution about nanoparticles were uniform, and that there was enough consistency throughout the scanned zone.

3.6. Applications of recombinant subtilisin

3.6.1. Biosurfactant activity

The purified recombinant protein subtilisin exhibited biosurfactant activities as determined through a screening assay known as oil spreading assay. Dispersion constitutes one of the features about biosurfactants utilized to recover trapped oil from oil wells. Fig. 5A and B demonstrates the power of the recombinant subtilisin and water as control to dissipate the film of burned motor oil, as demonstrated by the areas of clearness generated on the water's surface. According to Fig. 5A, no dispersion of oil was seen on water. The purified protein's surface activity was more widespread, with the measurement within the displaced ring being 7.5 cm and the accompanying circle area being 44.196 cm^2. (Fig. 5B).

3.6.2. Determinization of keratinolytic activity in dehairing of goat hide

The purified recombinant protein synthesized by *B. subtilis* displayed substantial stability up to for 24 h, therefore the protein's dehairing capacity was tested over each hour period, leading to the removal of small hairs from goat skin pelts. Within the first 4–5 h of exposure in the presence to recombinant subtilisin, just an adequate amount of hair was eliminated. The degree of hair removal, however, enhanced with a prolonged incubation time. Following 20 h of incubation, there was complete hair eradication. The outcomes suggest that purified recombinant subtilisin has greater hair removal properties despite the requirement to open hair pores. While the control group with buffer displayed no removal of hair easily as shown in Fig. 5C. Sensory evaluations, including touch and visual assessments, demonstrated how the skins dehaired by protein exhibited a white, softened, yet silky appearance with no obvious damage (Fig. 5D). On the contrary, the chemically processed skin seemed somewhat dark in shade, seemed tight when touched, and exhibited a coarse feature (data not shown).

3.6.3. Blood stain removal activity

The blood stain retrieval ability of the recombinant subtilisin was assessed by conducting experiments on cloth pieces stained with blood. The goal was to evaluate the protein's effectiveness in removing blood stains from the fabric. The outcomes for cloth pieces treated with different options are presented in Fig. 5E(a-d). Fig. 5E (a) showed the fabric treated with water as control. Detergent treatment alone (Fig. 5E (b)) showed modest stain removal performance compared to the protein treatment alone (Fig. 5E(c)). However, when the fabric had been subjected with a combination of detergent and recombinant protein, the stain was entirely eliminated as shown in Fig. 5E (d). This discovery reinforces the potential applications of purified protein in future industrial and biotechnological settings, particularly as a valuable bioadditive for enhancing cleaning efficacy in detergent formulations (Hadjidj et al., 2018).

3.6.4. Blood clot dissolution

The recombinant protein's influence on the breakdown of blood coagulation *in vitro* had been investigated. When water was employed for this assay, no evidence of blood clot dissociation was detected (Fig. 5F(a)). Within 4 h, recombinant subtilisin at 37 °C completely dissolved the blood clot. Fig. 5F(b) depicts the outcome. The protein successfully solubilized blood clots, and their dissolving rate increased with time. Within four hours, subtilisin effectively destroyed 91.08 % of the blood clots.

4. Discussion

The calcium alginate entrapment displays porosity and possess excellent mechanical stability, featuring functional groups that facilitate improved adsorption and, consequently, decrease the enzyme release from the support. The decline in the activity of the immobilized sample is due to the fact that whilst an enzyme clings to a transporter, its site of

action may become chemically occluded, leading to a disruption in the enzyme's proper interaction with its substrate (Mechri et al., 2022). When sodium alginate was utilized at the maximum concentrations of 4 and 4.41 % (w/v), the proteolytic yield of the immobilized protease fell dramatically. While the smallest dosage of 1.59 % (w/v) sodium alginate in solution resulted to have minimal proteolytic activity. In comparison to our study, many researchers have reported the optimal concentration of sodium alginate to be 2–3 % (Ismail and Sahimi, 2021). In a related literature, 4 % sodium alginate combined with 1 mL of purified protease from *Cheotomium globusum* has shown the highest relative activity of ~68 % while a decline in the activity was seen with increased protease concentration (Nadeem et al., 2020). The impact of concentrations of sodium alginate, varying between 1–3 % (w/v), on alkaline protease activity from *Bacillus amyloliquefaciens* SP1 was studied in a work reported by Guleria et al. (2016). The optimized calcium alginate concentration of 3 % revealed maximum activity for the stable formation of the immobilized bead. Different immobilization techniques have been reported to immobilize subtilisin-related proteins. For example, cellulose and nanocellulose are widely used in healthcare industries considering to their low level of toxicity, renewable nature, biological compatibility, and biodegradable properties. Laccase, lipases, glucose oxidase and pancreatic serine protease trypsin have been immobilized to various forms of cellulose material (Anirudhan and Rejeena, 2012; Wahba and Hassan, 2017). A literature study on cysteine proteases revealed the immobilization of bromelain, papain, and ficin on chitosan by adsorption technique to enhance the stability of all the enzymes used in the study (Holyavka et al., 2021). Another study on Carlsberg subtilisin produced by *Bacillus licheniformis* PB1 was immobilized on bentonite which is an inorganic matrix making it as a solid support substance, via adsorption approach (Rana et al., 2023). Subtilisin A was covalently coated on magnetic particles of silica with three amine binding agents: ATMS (brush-like linker), Jeffamine, and chitosan. ATMS-coated particles had the most amino groups on their surface, leading to the greatest protease activity among all systems evaluated as described by (Glomm et al., 2021).

Similarly, the immobilization of subtilisin-like serine protease from *S. mutabilis* strain TN-X30 (SPSM) using adsorption-encapsulation approaches with 3 various hybrid carriers revealed that the alginate-kaolin encapsulated SPSM beads has exhibited the best activity and proven to be stable at alkaline pH and high temperatures (Mechri et al., 2022). In a comparable immobilization investigation, the uncontrolled protease demonstrated maximal activity at 60 °C, whereas the most effective temperature for the protease immobilized onto chitosan, silica gel 100–200, alginate, glutaraldehyde-activated chitosan in addition to nitrocellulose membrane increased upto 70 °C. This phenomenon may arise from the immobilization process, which mitigates the steric barrier connecting enzymes and the substrates they digest in anticipation of both pH and temperature variations (Thakrar and Singh, 2019). A related study on Carlsberg subtilisin displayed an optimal temperature at 50 °C when immobilized with bentonite via adsorption, also it showed same optimal temperature for free enzyme. The influence of pH on the immobilized enzyme revealed at optimum level of pH 8 (Rana et al., 2023). The effect of immobilization on the stability of the enzyme is enhanced due to the enrichment of protein. This particular action might be attributed to a fluctuating entire charge across the protein junction. Enzyme surface charge dispersion improves binding to substrates and catalytic effectiveness, leading to higher level formation. The optimal pH value promotes the highest concentration of enzyme-substrate intermediates (Salis et al., 2007). Another proposed stabilizing process involves the formation of multifaceted covalent connections amongst the solid carrier and enzyme. The aforementioned links would stiffen the enzyme arrangement, causing the corresponding positions of the enzyme residues caught within the immobilization to remain secured despite the circumstances of the experiment, along with the sole permitted shifts would be determined by the length of the spacer arms. Such conformation rigidification might boost the stability of enzymes against distorting factors, such as elevated temperatures and solvents (Wahba, 2022).

The immobilization of AK-R protease on Ac-DMCSS-NH_2 nanospheres increased the enzyme's temperature maxima from 60 to 65 °C. The immobilized enzyme performed up to 3.0-fold better than the free enzyme throughout most temperature ranges evaluated. The immobilized AK-R protease's thermal stability improves due to multiple-point covalent attachment onto the mesoporous cover of DMCSS-NH_2 nanospheres. This stabilizes the enzyme's tertiary framework and conformational equilibrium within its active center, safeguarding it from thermal denaturation (A.S.S. Ibrahim et al., 2021).

Comparable findings have been documented following the immobilization of enzymes/proteins in gel beads made of alginate. A literature study showed the storage of soluble and immobilized alkaline protease from *Bacillus aryabhattai* Ab15-ES at 4 and 25 °C for 30 d which explained that the immobilized enzyme depicted relative activity to be at 80.88 % post 30 d while the free maintained at 64.6 %, at 4 °C. At ambient temperature, the free enzyme was completely inactivated while the immobilized alkaline protease secured 38.37 % of relative activity (Adetunji and Olaniran, 2023). Another research signifies the importance of storage of an immobilized neutral protease for a period of 11 d. It showed that there was > 80 % relative activity retained throughout the period and decrease was seen post 9th day. This decline has likely resulted from the swift reduction in storage stability induced by $CaCl_2$ and the liberation of soluble enzyme due to the degradation of gel beads. The immobilized enzyme, in this case, has likely utilized a substantial portion of the enzyme activity (Bai and Wu, 2022).

Similarly, a research cited by Qamar et al. (2020), depicted the reusability of calcium-alginate immobilized alkaline protease produced by *B. brevis* showed >60 % activity upto 10th cycle. A recent study of immobilized alkaline protease from *Bacillus aryabhattai* Ab15-ES exhibited >50 % relative activity upto 5th cycle and gradually decreased. The weakening of the bond between the matrix and the immobilized protein can lead to the physical detachment of enzyme off the supporting substance. Moreover, the decline in enzyme activity may occur as a consequence. Moreover, with successive use, the pore size of the alginate beads expands, resulting in heightened protein leakage and a subsequent decrease in biocatalytic activity (Adetunji and Olaniran, 2023). The functioning of the immobilized pair of beads was assessed six times consecutively in a study on the usability of immobilized strawberry protease. It was noted that 62 % of the activity remained preserved in the third usage of the immobilized beads, whereas there was a significant decline in the performance after the fourth reuse (Alici and Arabaci, 2024). A similar study on immobilized protease depicted the reusability of beads at 4 °C and 26 °C until 4 days where immobilized beads showed more stability at 26 °C. The reason for decreased activity in the immobilized beads post second day is because of the damage caused to the beads for repeated usage (Nina Vanessa et al., 2022).

An identical study indicated that the protein SLSP-k demonstrated 90 % activity following treatment using 0.5 % Tween 20 and 1 % Triton X 100, whereas it displayed 70 % while administered 0.5 as well as 1 % SDS (Gurunathan et al., 2021). Another research completely verifies our results, stating the enzyme proved highly stable in with the addition of surfactants that are not ionic notably Triton X-100, Tween 20, Tween 80, and anionic surfactants like SDS (Ding et al., 2020). A report by Marathe et al. (2018), suggested that Tween 20 has shown the highest protease activity for immobilized alkaline protease, than SDS and Triton X-100 respectively which also coincides with our results of immobilized subtilisin. In a related literature, SDS has shown very less relative activity on entrapped lipase from H1 (*P. reinekei)* and H3 (*P. brenneri*) (Priyanka et al., 2019). In contrast, 1 % SDS and Triton X-100 has heightened the relative activity of immobilized alpha amylase from *A. pullulans* at 110 % and 114 %, whereas similar results to ours are shown for Tween 80 (Nelson Ademakinwa et al., 2021). Strawberry protease has been discovered to be relatively stable in an environment of surfactants that are nonionic. Brij 35 had essentially little effect on the function of both

free and immobilized strawberry proteases as compared to the control group. Moreover, in the presence of hydrogen peroxide, activity of enzymes fell to half thereby resulting in slight difference between free and bound protease (Alici and Arabaci, 2024).

In a related work, the hydrolytic activity of SLSP-k demonstrated an increase amidst trace metals, including Ca^{2+}, Co^{2+}, Li^{2+}, Mg^{2+}, Mn^{2+}, and Zn^{2+} (Gurunathan et al., 2021). The disparity in protein activity when exposed to metal ions is determined by the amount of every ion of metal inside cells and organelles, which falls within a certain range specified by the biological environment. An investigation was conducted to examine the impact of ions on the activity of unbound and CHI-immobilized protease from *Cheotomium globusum*. Results revealed that Ca^{2+}, Mg^{2+} exhibited stimulatory effects, while K^{+} showed no influence on enzyme activity (Nadeem et al., 2020). Our investigations are in consistent to the previously reported findings. But very less literature is available on the research of immobilized recombinant subtilisin when treated with metal ions. Other researchers have assessed the Calcium ions to be enhancing the relative activities of immobilized enzymes when compared to free and this goes in line with the present study (Abdella et al., 2023; Nelson Ademakinwa et al., 2021) have reported that $CaCl_2$ and Ca^{2+} have displayed enhancing ability of the immobilized enzymes of protease from *Bacillus thuringiensis* strain-MA8 and alpha amylase from *A. pullulans* at ~140 % and 119 % respectively. KCl has slightly displayed lesser relative activities for immobilized enzymes than the free enzymes (Abdella et al., 2023; Priyanka et al., 2019).

Similar results have also been found which states that EDTA signifies the catalytic activity in calcium alginate immobilized beads with enzymes (Abdella et al., 2023; Karim et al., 2017; Thakrar and Singh, 2019). In our study, the free and immobilized subtilisin exhibited stability and retained 90.78 % and 92.08 % activity respectively, in the presence of 1 M DTT as shown in Table 1. Conversely, β-mercaptoethanol demonstrated nil significant impact on the activity of protease, indicating that the enzyme lacks vital disulfide bonds. In consistent to our study, PMSF has inhibited purified AprE127 subtilisin produced from *B. subtilis,* as it is a prominent serine protease inhibitor (Frias et al., 2021; Mechri et al., 2019).

A literature referenced by Ding et al. (2020), with the exception of isopropanol, all tested organic solvents like acetone, ethanol, methanol and DMSO in the range of 20–40 % exhibited an enzyme activity level ranging from approximately 86 % to 133.6 % of its original activity, indicating a remarkable tolerance to organic solvents by recombinant subtilisin-like protease (mAls). Furthermore, Farhadian showcased a extracellular htrA-like serine protease by *Bacillus subtilis* 16 DR8806, which demonstrated an enhancement in activity when exposed to methanol and ethanol (Farhadian et al., 2015). Similar research works have reported the impact of organic solvents on the immobilized enzymes. Priyanka et al. (2019) investigates in their study and showed that methanol and ethanol at 10 % each, when subjected to entrapped lipases from H1 (*P. reinekei*) and H3 (*P. brenneri*) displayed loss of activity when compared to free lipase at 28 °C with 91.12 % and 99.64 (methanol) and 76.41 % and 73.45 % (ethanol) respectively for the latter. Non-polar solvents are renowned for being capable of adhering to the lipase lid, retaining the lipase in a relaxed state and so improving lipolytic activity; nonetheless the entrapment mechanism may hamper this association by diminishing structural flexibility. Due to the restricted movement of the enzyme within the alginate beads, non-polar solvents are unable to interact with the enzyme lid, resulting in the observed activation of lipolytic activity. Ethanol showed stability in both free and calcium alginate immobilized endo (1 → 4) β-d-glucanase with ~ 99 % while methanol increased by 1.13 folds in case of immobilized enzyme (Karim et al., 2017). Another literature study investigated the implications of organic solvents affecting the immobilized lipase (IL) activity of *Burkholderia cepacia* which states that chloroform revealed 80 % residual activity at 120 h (Padilha et al., 2018) while it showed 1.21 fold enhancement in the activity of endo (1 → 4) β-d-glucanase when immobilized with calcium alginate (Karim et al., 2017). The reduction in water content around a catalytic site serves as a typical illustration of a decline in activity observed in an immobilized enzyme upon exposure to a solvent.

Similarly the increase in K_m and decline in V_{max} values of free SPSM and immobilized forms of subtilisin-like serine protease from *S. mutabilis* strain TN-X30 SPSM, with casein and Suc-F-A-AF-*p*NA substrates, verifies the specificity of the substrate required to transform a product in per unit time (Mechri et al., 2022). The specificity of substrates of thermoresistant serine alkaline protease from *Aeribacillus pallidus* C10 displayed heightened action in the company of casein with 100 % (Yildirim et al., 2017). The proteolytic efficacy of both variants of protease was evaluated under the influence of various substrates of protein (1 % w/v), encompassing transferrin, hemoglobin, albumin, ɣ-globulin, and casein. Fibrin was utilized as the substrate, with its protease activity considered as 100 %. The outcomes revealed that the unbound and immobilized proteases exhibited 2.44 and 4.05 times greater activity compared to the control when albumin was present (Badoei-dalfard et al., 2020). In a related cited work, proteolytic activity of fibrinolytic enzyme on different substrates revealed that casein and serum albumin displayed 3.2 times and 6.4 times greater activities respectively, than control fibrin (Krishnamurthy and Belur, 2018). In contrast, both native KBALT and recombinant KBALT, keratinase from *Bacillus altitudinis* RBDV1, demonstrated a substrate preference for chicken feather, with subsequent affinities for keratin azure, human hair, and human nail followed by comparatively least specific towards BSA and casein (Pawar et al., 2018).

The kinetic parameters of the purified extracellular alkaline protease from *Bacillus licheniformis* K7A (SAPHM) showed greater catalytic efficiency towards the specific synthetic substrate Suc-Phe-Ala-Ala-Phe-*p*NA than casein in comparison to commercially available substrates Alcalase and Thermolysin (Hadjidj et al., 2018). In line with our investigations, another research study has investigated the kinetic parameters as follows- the K_m and V_{max} values for the soluble enzyme (alkaline protease produced by *Bacillus brevis*) were measured at 0.19 μM and 333.3 U/mL, respectively. In contrast, for the calcium-alginate immobilized enzyme, the K_m was reduced to 0.09 μM, and the V_{max} increased to 454.5 U/mL. These findings are consistent with current investigation. The association involving an amount of the substrate and the enzyme synthesis demonstrated that the enzyme that had been immobilized had a higher specificity towards the substrate than the unbound protease in solvent. The process of immobilization induced modifications in the enzyme's active site, subsequently leading to a decline in the K_m point of the enzyme which reflects a stronger binding between the protein and substrate molecules. The elevated V_{max}, diminished K_m values, and enhanced pH and thermo-resistibility of the enzyme immobilized in Ca-alginate render it a resilient catalyst applicable across various industrial domains, notably in sectors such as textiles and detergents (Qamar et al., 2020). A study on protease revealed that, BSA digestion at 40 °C and a pH of 6 yielded K_m and V_{max} values of 0.041 mm and 2.48 μmol tyrosine $mL^{-1}min^{-1}$ with unbound crude strawberry protease, along with 0.089 mm and 2.47 μmol tyrosine $mL^{-1}min^{-1}$ regarding immobilized crude protease enzyme, respectively. The rise in protease's value of K_m for the BSA substrate might be attributed mostly to diffusion issues (Alici and Arabaci, 2024). In consistent to the current study, the immobilized alkaline protease from *Bacillus aryabhattai* Ab15-ES exhibited a calculated K_m of 1.225 mg/mL, which is lower than the K_m value of 2.023 mg/mL for the free enzyme. This decreased Km value suggests a 1.65-fold improvement of the enzyme's attraction towards the base after being immobilized in alginate gel pellets. Furthermore, the Vmax of the attached protease (250 U/mL) surpassed the value of the enzyme in free form (232.56 U/mL), indicating a more effective configuration of this enzyme within the solid substrate (Adetunji and Olaniran, 2023). Another kinetic study of immobilized α-amylase indicated that the immobilized enzyme exhibited lesser K_m and V_{max} values when compared to the soluble form, thereby depicting increase in the enzyme activities post immobilization

(Al-Harbi and Almulaiky, 2020).

Nanotechnology has gained popularity over the past few decades as a consequence of the manufacturing and development of nanoscale substances. The synthesis of nanoparticles (NPs) is a developing feature of nanotechnology. In line with the outcomes of the current investigation, Sidhu and Nehra, (2021) have reported the generation of Bac23-capped silver nanoparticles (SNPs) with a characteristic peak at 432 nm. In a separate study, Guilger-Casagrande et al. (2021) similarly reported an absorption peak for biogenic nanoparticles with the filtrate of *Trichoderma harzianum*, between 400–420 nm. Aligned with the outcomes of the present study, other results were predominantly consistent, affirming the application of the ultraviolet–visible spectroscopy method to establish the existence of lipopeptides of *B. subtilis* SDUM301120 over the outermost layer of silver nanoparticle. The absorption spectrum revealed peaks within 430–460 nm range, indicating specificity and contributing to the heightened antibacterial effectiveness (Yu et al., 2021). Several other metal oxides have been studied in the capping of proteins. The report examines the manner in which nickel oxide nanoparticles employed in diverse industries affect the activity of Neutrase 1.5MG, a proteolytic enzyme, and laboratory mashing of light barley malt, as explained by (Karpenko and Kanaev, 2021). Mucolytic enzymes, including papain (PAP) and bromelain (BRO), were covalently attached to poly acrylic acid (PAA). The ionic gelation process was then used to create nanoparticles (NPs). Among them, NPs conjugated with BRO displayed highest functionalities in drug delivery systems for mucus permeation (Pereira de Sousa et al., 2015).

In a citation reported by Ahmed et al. (2022), the eco-friendly production of zinc nanoparticles was examined to assess its impact on the harvest and development regarding *Pisum sativum* L. An evident spike at 374 nm had been identified, signifying the generation of white-coloured nanomaterials. A work documented by Hosseini-Koupaei et al. (2019) explored the relationships and longevity of proteinase K, a serine protease which is subtilisin-like, in an environment consisting of CuO (copper oxide) nanomaterials having a 270 nm spectral peak. The study's results have far-reaching ramifications in medical science, biology, and a variety of commercial possibilities. The existence of the small spike implies that the manufactured zinc oxide nanoparticles have an elevated degree of consistency and standardization, indicating a painstakingly managed biosynthesis approach. The distinctive peak for ZnONP derived from the *Phragmanthera austroarabica* extract manifested at 362 nm, signifying emergence of nanomaterials. Following a 4-hour incubation period, there was a partial increase in the solution's absorbance. Nevertheless, the solution's color remained constant, and the level of absorption sustained stability even after 24 h. The steady absorption over an extended period indicates the conclusion of the process, achieving the successful diminution of Zn^{2+} ions into nanoparticles of zinc (ZnNP) (Alahdal et al., 2022). The bioconjugate nano-silver enzyme complex BC-nAg-Akp production was optimized with an acetone solution. Silver nanowires happen to have been synthesized using extracellular protease-resistant fibrillar proteins extracted from an acetone-concentrated enzyme solution, thereby increasing the activity of alkaline protease (Akp) enzyme due to nanoparticle interaction (Joshi et al., 2020). The protease produced from *Pseudomonas aeruginosa* and *Enterococcus hirae* was attached to magnetic nanoparticles through surface conversion technology, incorporating silica bound magnetic nano combination, amine and cysteine functioned in nano composite production. The study proved that there was increase in the activity and stability of the enzyme via nanoparticle conjugation (Masi et al., 2018).

A boost in activity was additionally observed against food-borne pathogens when silver nanoparticles were incorporated with bacteriocin Bac23 extracted from a lactic acid bacterium (*Lactobacillus plantarum* PKLP5) (Sidhu and Nehra, 2021). Another research studied the antibacterial activity of nanoparticles which aided in an effective wound healing application. The unique characteristics of small-sized AgNPs, in conjunction with their broadened surface area, promote effective contact between them and the affected wound covering, hence decreasing scar-healing time. The highest effectiveness was evident against multidrug-resistant (MDR) *P. aeruginosa* isolates (20–25 mm) and *E. coli* (18–22 mm) (Gomaa, 2019). Similarly, silver nanoparticles derived from *Selaginella bryopteris* (commonly addressed sanjeevani) plant extract (SPE@Ag-NPs) had significant antibacterial properties against *S. aureus* (11 mm) and *E. coli* (12 mm) than *Selaginella* plant extract (SPE) alone (S.S. et al., 2019). AgNPs are more effective against bacteria while being less hazardous to humans. Ag ions tend to be coupled to negative-power biomolecules including RNA, DNA, and protein molecules. Silver nanoparticles generated by biological techniques possess antibacterial efficacy against microbes, such as methicillin-resistant *Staphylococcus aureus (S. aureus)* (Elizabeth et al., 2022). The production of nanoparticles of silver and their effects against the infection caused by bacteria *V. cholera* has also been investigated. While antibacterial drugs are utilized, modifications to membrane permeability and reciprocal silver nanoparticle accessibility in microbial cells are currently described in recent times (Bamal et al., 2021).

A recent study has depicted a good antibacterial activity of zinc oxide nanoparticles conjugated with *W. volbulis* plant extract by agar well diffusion assay, against S. *epidermis* and *E. aerogenes* with 16 mm and 10 mm respectively. The present study has also shown greater activity against Gram-positive bacteria (Jeyabharathi et al., 2022). Subtilisin has more efficacy against *S. aureus* (10.3 μM) than against *E. coli* (15.6 μM), indicating that it acts more effectively on the peptidoglycan coating of Gram-positive microorganisms rather on the lipopolysaccharide covering of Gram-negative microorganisms. Conjugation of AuAgNP with subtilisin increases the former's effectiveness against *S. aureus* but inhibits its activity against *E. coli* as reported by (Prabhawathi et al., 2019).

The antioxidant assay employs the stable radical DPPH to gauge the ability of an antioxidant to counteract free radicals, offering valuable insights into the substance's potential antioxidant characteristics. As previously mentioned by Iqbal et al. (2017), the ability to reduce DPPH decreases with increasing concentrations of the extract. Maximum scavenging activity of methanol extract of *D. stramonium* was found to be 64.28 % at 60 μg/mL concentration. Another report studied the antioxidant activity using DPPH assay wherein the *Datura inoxia* Mill. (Solanaceae) methanolic leaf extract's potential to scavenge free radicals revealed 82 % inhibition at 1.0 mg/ml (Bagewadi et al., 2019). Selenium nanoparticles (SeNPs) produced by *B. subtilis* BSN313 at 24 and 48 h exhibit good antioxidant activity by DPPH and ABTS methods (Ullah et al., 2021). In contrast to another literature, the antioxidant activity of the biosynthesized selenium nanoparticles produced by *Bacillus* species showed no significant result in the DPPH assay (Greeshma and Mahesh, 2019).

Antioxidant nanoparticles possess the potential to increase medicinal efficacy by shielding them against oxidative destruction or inactivation. When medications are encapsulated within antioxidant nanoparticles, its durability as well as accessibility inside the human body is improved, resulting in enhanced therapeutic outcomes. In a previous study, Given the same dose as DPPH (150 μg/mL), the ABTS free radical scavenging capability of SeNPs was determined to be 63.01 and 60.61 %, respectively, after 24 and 48 h (Ullah et al., 2021). Another researcher explains the ABTS activity of biosynthesized silver nanoparticles by ABTS method. The proportion of inhibition progressively rises as time passes, reaching its highest level between 16 and 40 min (S. Ibrahim et al., 2021). A recent research employing wild subtilisin from *B. subtilis* strain ZK3, in combination with nanoparticles of silver and zinc oxide that revealed strong antiradical action, with ZnONP exhibiting maximal inhibition of 90 % and AgNP of 45 % at 60 h (Shettar et al., 2023a). Nanoparticles (NPs) can be utilized to prevent, diagnose, and cure a variety of illnesses due to their tiny size, huge surface area, and distinctive structure. They can also improve medication biodistribution and release in regulated ways (Oshi et al., 2022; Patra et al., 2018). In a literature study of aqueous extract of loquat seed (AELS), the high relationship between antioxidant activity and NP concentration suggests

that tiny ZnO NPs with a wide surface area may contribute to their antioxidant ability. However, increasing the number of active sites on generated ZnO NPs may increase the effectiveness of their antioxidants (Shabaani et al., 2020).

Silver nanoparticle cytotoxicity varies considerably depending on particle form and production technique, since it is affected by parameters such as exposure period, temperature, concentration, size of particles, capping, and the specific cell line used. A research investigation demonstrated that the methanolic extract of the seeds of *D. stramonium* proved cytotoxic against breast adenocarcinoma (MCF-7) lines of cells, having an the IC_{50} value of 113.05 μg/mL (Iqbal et al., 2017). Another work on anticancer properties of nanoparticles revealed that the animal cohorts subjected to bacteriocin and AgNPs displayed survival rates of 82.56 % and 62.33 %, respectively. The amalgamation of bacteriocin with AgNP resulted in a reduction of AgNP toxicity (Gomaa, 2019). The crude extract and its fraction from Brazilian Red Propolis (BRP) exhibited a pronounced cytotoxic effect. Similarly the biosynthesized AuNP (gold nanoparticles) revealed highest dose-dependent cytotoxic effect among all the other nanoparticles studied against bladder cancer cells (T24) and prostate cancer cells (PC-3) as reported by Botteon et al. (2021). A report on the conjugation of nanoparticles on mucolytic enzymes papain (PAP) and bromelain (BRO) were studied for cytotoxic studied revealing the polymers and conjugated nanoparticles to be non-toxic at all concentrations when tested against Caco-2 cell lines (Pereira de Sousa et al., 2015). Multiple kinds of nanomaterials made of inorganic substances and ways for producing these have enabled the manipulation of novel drug delivery systems. Before turning these inorganic nanoparticles into therapeutic compounds, several important considerations must be made. distinguished in comparison to better-organized nanoparticles that organic, the therapeutic transformation of inorganic nanomaterials for the delivery of drugs continues to remain under debate due to a lack of greater evidence and information on biological safety, particularly bio-catalytic attributes, elimination techniques, and long-term toxicological assays that demonstrate its *in vitro* and *in vivo* biological security (Oshi et al., 2022). Because of their low systemic toxicity, AgNPs can be used to target specific cancer vulnerabilities. Several research revealed the positive function of AgNPs in the treatment of cancer (Gurunathan et al., 2015). Another study discovered that treatment with AgNPs derived from *Butea monosperma* leaf extract significantly inhibited cancer cell lines (B16F10, A549, MCF7, and HNGC2F) (Patra et al., 2015). The toxicity of AgNPs on ovarian carcinoma stem cells was examined, and the results indicated that A2780 and ALDH+/CD133+ colonies were greatly decreased (Choi et al., 2016).

Similar outcomes were tabulated regarding a biosurfactant produced by *B. velezensis* KLP2016 with RT at 1.130 min. The standard surfactin showed a peak at RT 1.27 min (Meena et al., 2021). In consistent to our results, a study reported by Barale et al. (2022), displayed a chromatogram with 2 peaks at RT 2.91 min, 4.02 min, 5.47 min, and 6.8 min. This goes in line with the standard surfactin used showing its homologues at 2.61 min, 3.0 min, and 4.20 min. Hence, the purified recombinant subtilisin seemed to be a molecule akin to surfactin.

The distinctive absorption bands in AgNP spectra of FTIR provide essential details concerning the molecular makeup and architecture of generated nanoparticles, enabling researchers to gain insight into the biomolecules that comprise the procedure for synthesis. Comparable stretches and peaks have been identified in numerous literary works. The strong connections among water ions and nanoparticles are anticipated to play a substantial part in stabilizing and promoting biomolecule bonding on AgNP surfaces throughout the course of production. In the identical work, specific peaks with minor alterations have been noticed in nanoparticles made of silver produced by *B. subtilis* (A15) (Fouad et al., 2017). The results indicate hydroxyl sections, C–C-O categories, and amide sequences are vital components involved in minimizing and stability of Bac23-capped SNPs. The results presented here strongly demonstrate the existence of bacteriocin proteins that engaged during the formation as well as encapsulation within the nanostructures (Sidhu and Nehra, 2021). The FTIR spectrum of absorption of the biosurfactants generated by *B. amyloliquefaciens* SAS-1 and *B. subtilis* BR-15 explained the presence of peptides, an aliphatic, an ester, and carbonyl chains, verifying the existence of lipopeptides. Similar bands were observed in the current investigation (Sharma et al., 2018). The existence of magnetic nanoparticles combined with alkaline protease, bearing a shell made of silica were confirmed by a distinctive adsorption peak at 1090 cm^{-1}, indicating the presence of silane groups. A sample with a double coating of silica-amino silane reveals a region of both materials (Masi et al., 2018).

A further study on the formation of nanoparticles formed of zinc oxide that was produced by biosynthesis from *P. austroarabica* extract revealed likely peaks and shown that they play a vital component in lowering the number of Zn ions and operate as protective coverings for nanomaterials made of zinc oxides (Alahdal et al., 2022). The FTIR spectra of assynthesized and lipase immobilized ZnO nanoparticles revealed characteristic ZnO peaks beyond 600 cm^{-1}, assessing the existence of ZnO material. The amide bond spikes, regardless of side groups, mirror the composition of the core polypeptide strand. These additional bands were associated with nanoparticle modification and immobilization of lipase (Khan et al., 2019). Similar bends and stretches were also found in the FTIR spectra of the current research work, thereby correlating and confirming the presence of functional groups of nanoparticles made of zinc oxide bound with recombinant subtilisin.

Based on the SEM-EDS outcomes for recombinant subtilisin bound nanoparticles, the current study verifies the arrangement and fundamental makeup of the resultant nanoparticles in contrast to earlier research. A recent study also illustrated a scanning electron microscopy photograph of a dehydrated amount of silver nanoparticles (AgNPs) with a median size of 50 nm and a shape that is spherical produced from *B. subtilis* NCIB 3610 culture supernatant. (Omole et al., 2018). Similar findings were observed from zinc nanoparticles made from *P. austroarabica*, that demonstrated an abundance of metals as well as the availability of carbon, suggesting that phytochemicals contribute in reducing and capping the amount of biosynthesized ZnONPs (Alahdal et al., 2022). The abundance of bioconjugate nano-silver enzyme in the fundamental state of silver was confirmed by SEM-EDS analysis having small sized agglomerated embedded with alkaline protease (Akp). The proportion by weight and atomic ratio of silver reported to have values of 18.32 % and 3.79 %, respectively (Joshi et al., 2020).

The outcomes align closely with the results obtained in the present investigation of recombinant subtilisin-capped AgNP. In a comparable circumstance, chitosan polymeric-coated mesoporous nanoparticles of silica demonstrated a reduction in weight of 28.8 %, whereas the polymer alone exhibited an even greater weight reduction of 68.9 % (Özbek and Ünal, 2017). The weight reduction, reaching until 60 % in the temperature range of 300–400 °C, was attributed to the breakdown of organic constituents. This study described the environmentally friendly manufacture of nanoparticles of silver utilizing the leaves of *Aquilegia pubiflora.* This research was documented by Jan et al. (2021). In a correlated investigation performed by Alam (2022), the heat resistance of silver nanoparticles biosynthesized from strawberry fruit pomace extract was assessed through TGA in a nitrogen environment. The silver nanoparticles exhibited a weight stability of up to 75 %. Based on the results of analogous studies on nanoparticles conducted by other researchers, it is indicated that nanoparticles capped with purified recombinant subtilisin exhibit commendable thermal stability, and these observations have been relatively underreported.

The outcomes from the present research work of recombinant subtilisin conjugated with nanoparticles (Ag and ZnO) indicated a round-like and rough morphology, aligning with reports from other research studies in the literature. In a similar investigation, the pictures of ZnO nanoparticles from *B. subtilis* demonstrated surface roughness with an even distribution (Fazaa, 2022). A research explained by Guilger-Casagrande et al. (2021) shared his findings stating that the uncapped nanoparticles had greater average dimensions in AFM photographs,

however capped nanoparticles possessed a circular morphology. The geometry and dimension of the silver nanoparticles were validated utilizing AFM. With a particle size of around 50 nm, symmetrical, spherical nanoparticles were spread equitably (Kabeerdass et al., 2021). Nanoparticles (NPs) can enhance the bioavailability of weakly water-soluble medicinal products and deliver them to specific areas in the body, reducing unwanted effects. Nanoparticles (NPs) can transcend physiological barriers as well as intercellular gaps because of their tiny size (Patra et al., 2018).

The oil displacement area of a biosurfactant molecule generated by a native strain of *A. niger* (2.3 g/L) was 49.74 cm^2 whereas the mutant strain showed 59.81 cm^2 (Asgher et al., 2020). (Pele et al., 2019) identified a crude biosurfactant generated from *R. arrhizus* UCP1607 exhibiting a 53.4 cm^2 oil displacement area (ODA) dispersing effect. In consistent to the current study, (POOMTIEN et al., 2013) additionally discovered that the dispersion rate equivalent to 44.5 cm^2 ODA for *Cyberlindnera samutprakarnensis* JP52 biosurfactant. The biosurfactant derived from *Ochrobactrum anthropi* HM-1 culture exhibited elevated surface activity, evident in a displaced circle with a 7 cm diameter and a corresponding circle area of 38.5 cm^2. The biosurfactant from *Citrobacter freundii* HM-2 produced a distorted circular that had a slightly smaller dimension of 6.5 cm and a surface area of 33.17 cm^2 (Ibrahim, 2018). In this present research, the biosurfactant activity of purified recombinant subtilisin was demonstrated, showcasing its potential for application in oil recovery processes.

The dehairing process has garnered significance as an alternative to chemical technique in the contemporary scenario. This technique plays a crucial role in reducing toxicity while simultaneously enhancing the quality of leather by using biomolecules instead of commercial chemicals. Keratinolytic studies demonstrated that hair from goat skin may be effortlessly removed 24 h after exposure with alkaline protease from *Bacillus* sp. contrasted to skin treated merely with buffer (control). This demonstrates the protease's keratinolytic activity (Kandasamy et al., 2018). In a related study reported by Hussain et al. (2017), upon 12 h of incubation, the enzyme had removed part of the hair from the chicken quill. The findings revealed that alkaline protease of *B. subtilis* served as a better hair remover that had no effect on opening the hair openings. In a prior investigation, skin slices from goats possessed dehairing via alkaline protease generated by the fungal strain *Neocosmospora* spp. N1. The technique was juxtaposed with a traditional chemical method which employs limestone and sulfide, which is frequently utilized in the leather goods sector. Hairs were readily removed in contrast with the control during 24 h of incubation while utilizing enzymatically and chemically processed skin (Matkawala et al., 2019).

Numerous reports have emphasized the usefulness of proteases having alkaline property for assisting eliminate stains of blood from cotton material. The information depicted in a research study by Hadjidj et al. (2018), demonstrates that the isolated and purified extracellular alkaline protease from *Bacillus licheniformis* K7A (SAPHM) remains exceptionally stable and compatible with all examined solid laundry detergents, maintaining 100 % of its original activity when incubated at 40 °C. Blood stains were partly erased in with the addition solely of detergent and enzyme. However, a blend of detergent and purified enzyme succeeded in total elimination of blood stains after twenty minutes of incubation at 15 °C. Other researchers have discovered cold-active proteases generated from diverse microbial species as viable options for low-temperature detergent manufacturing (Furhan et al., 2019). After 10 min of incubation utilizing the optimized protease of *B. subtilis* with the addition of a detergent, (Hussain et al., 2017) claimed that the blood stain had been eliminated entirely from a cotton fabric piece. Our findings indicate that the recombinant subtilisin protein derived from *B. subtilis* exhibits superior effectiveness. The results presented here highlight the protein's potential for eventual application for a disinfectant bioadditive in detergent for laundry formulations.

In a related study, a fibrinolytic enzyme (serine protease) named ACase from mushroom efficiently dissipated the blood clots and rate of dissolution increased as time progressed. Within a span of 3 h, the enzyme managed to dissolve 82 % of the blood clots (Li et al., 2021). A complete blood clot solubilization within 4 h at 37 °C had been determined by a study conducted by Sharma et al. (2019), in which a fibrinolytic protease from *B. cereus* RSA1 was utilized. A protease coming from *M. oleifera* Lam illustrates plasmin-like function in clotting blood dissolution under *ex-vivo* as well as *in-vitro* breakdown of fibrin (Sawetaji, 2023).

5. Conclusion

In this ongoing investigation, recombinant subtilisin has been embedded in Ca-alginate beads by altering the variables for enhanced functional resilience. It emerged that the use of suitable gelling agent and the amount of protein alters the location of the catalytic process by boosting enzyme activity. Analysis revealed that alginate immobilization enhances the performance and endurance of entrapped subtilisin throughout an alkaline pH spectrum (9–11) and heat tolerance at 80 °C. The immobilized protein's excellent efficacy in all biochemical processes and recyclability potential imply a high economic worth. The biological features of the recombinant subtilisin-capped Ag and ZnO nanoparticles revealed antibacterial, antioxidant, and cytotoxic capabilities. The thermostability of nanoparticles was demonstrated by fundamental, surface, and multifunctional attributes. Nevertheless, the industrial utilization of recombinant protein, known for its elevated temperature and pH stability, such as in dehairing, blood clot dissolution, biosurfactant property and blood stain removal demonstrates positive effects on both human well-being and the environment. The research sheds light on the potential applies of entrapped recombinant subtilisin and its nanoparticles for intriguing biological activities in healthcare and environmental sector.

CRediT authorship contribution statement

Shreya S. Shettar: Writing – original draft, Visualization, Validation, Methodology, Investigation, Conceptualization. **Zabin K. Bagewadi:** Writing – review & editing, Writing – original draft, Supervision, Resources, Project administration, Data curation, Conceptualization. **T. M. Yunus Khan:** Writing – review & editing, Formal analysis. **Shaik Mohamed Shamsudeen:** Writing – review & editing, Funding acquisition. **Harsh N. Kolvekar:** Methodology, Investigation.

Declaration of competing interest

The authors declare that they have no known competing financial interests or personal relationships that could have appeared to influence the work reported in this paper.

Acknowledgements

The authors extend their appreciation to the Deanship of Scientific Research of King Khalid University, Abha, Kingdom of Saudi Arabia for funding this work through small research groups. RGP. 1/214/45. The authors acknowledge KLE Technological University, Hubballi, for support through the Ph.D. Fellowship Program.

References

Abdella, M.A.A., Ahmed, S.A., Hassan, M.E., 2023. Protease immobilization on a novel activated carrier alginate/dextrose beads: improved stability and catalytic activity via covalent binding. Int. J. Biol. Macromol. 230, 123139 https://doi.org/10.1016/j.ijbiomac.2023.123139.

Adetunji, A.I., Olaniran, A.O., 2021. Production and potential biotechnological applications of microbial surfactants: an overview. Saudi J. Biol. Sci. 28, 669–679. https://doi.org/10.1016/j.sjbs.2020.10.058.

Adetunji, A.I., Olaniran, A.O., 2023. Biocatalytic profiling of free and immobilized partially purified alkaline protease from an autochthonous *Bacillus aryabhattai* Ab15-ES. Reactions 4, 231–245. https://doi.org/10.3390/reactions4020013.

Ahmed, S., Qasim, S., Ansari, M., Shah, A.A., Rehman, H.U., Shah, M.N., Ghafoor, U., Naqvi, S.A.H., Hassan, M.Z., Rehman, S. ur, Ahmad, F., Shoaib, S., Alahmadi, T.A., Alharbi, S.A., Datta, R., 2022. Green synthesis of zinc nanoparticles and their effects on growth and yield of *Pisum sativum*. J. King Saud Univ. - Sci. 34, 102132. Doi: 10.1016/j.jksus.2022.102132.

Akhtar, M.S., Panwar, J., Yun, Y.-S., 2013. Biogenic synthesis of metallic nanoparticles by plant extracts. ACS Sustain. Chem. Eng. 1, 591–602. https://doi.org/10.1021/sc300118u.

Alahdal, F.A.M., Qashqoosh, M.T.A., Manea, Y.K., Salem, M.A.S., Khan, A.M.T., Naqvi, S., 2022. Eco-friendly synthesis of zinc oxide nanoparticles as nanosensor, nanocatalyst and antioxidant agent using leaf extract of *P. austroarabica*. OpenNano 8, 100067. https://doi.org/10.1016/j.onano.2022.100067.

Alam, M., 2022. Analyses of biosynthesized silver nanoparticles produced from strawberry fruit pomace extracts in terms of biocompatibility, cytotoxicity, antioxidant ability, photodegradation, and *in-silico* studies. J. King Saud Univ. - Sci. 34, 102327 https://doi.org/10.1016/j.jksus.2022.102327.

Al-Harbi, S.A., Almulaiky, Y.Q., 2020. Purification and biochemical characterization of Arabian balsam α-amylase and enhancing the retention and reusability via encapsulation onto calcium alginate/Fe2O3 nanocomposite beads. Int. J. Biol. Macromol. 160, 944–952. https://doi.org/10.1016/j.ijbiomac.2020.05.176.

Alici, E.H., Arabaci, G., 2024. Strawberry protease as a laundry detergent additive candidate: immobilization, compatibility study with detergent ingredients, and washing performance test. Glob. Challenges 8. https://doi.org/10.1002/gch2.202300102.

Anirudhan, T.S., Rejeena, S.R., 2012. Adsorption and hydrolytic activity of trypsin on a carboxylate-functionalized cation exchanger prepared from nanocellulose. J. Colloid Interface Sci. 381, 125–136. https://doi.org/10.1016/j.jcis.2012.05.024.

Asgher, M., Arshad, S., Qamar, S.A., Khalid, N., 2020. Improved biosurfactant production from *Aspergillus niger* through chemical mutagenesis: characterization and RSM optimization. SN Appl. Sci. 2, 966. https://doi.org/10.1007/s42452-020-2783-3.

Ashokbhai, J.K., Basaiawmoit, B., Das, S., Sakure, A., Maurya, R., Bishnoi, M., Kondepudi, K.K., Padhi, S., Rai, A.K., Liu, Z., Hatia, S., 2022. Antioxidative, antimicrobial and anti-inflammatory activities and release of ultra-filtered antioxidative and antimicrobial peptides during fermentation of sheep milk: *In-vitro, in-silico* and molecular interaction studies. Food Biosci. 47, 101666 https://doi.org/10.1016/j.fbio.2022.101666.

Badoei-dalfard, A., Khankari, S., Karami, Z., 2020. One-pot synthesis and biochemical characterization of protease metal organic framework (protease@MOF) and its application on the hydrolysis of fish protein-waste. Colloids Surf. B Biointerfaces 196, 111318. https://doi.org/10.1016/j.colsurfb.2020.111318.

Bagewadi, Z.K., Mulla, S.I., Ninnekar, H.Z., 2017. Purification and immobilization of laccase from *Trichoderma harzianum* strain HZN10 and its application in dye decolorization. J. Genet. Eng. Biotechnol. 15, 139–150. https://doi.org/10.1016/j.jgeb.2017.01.007.

Bagewadi, Z.K., Muddapur, U.M., Madiwal, S.S., Mulla, S.I., Khan, A., 2019. Biochemical and enzyme inhibitory attributes of methanolic leaf extract of *Datura inoxia* Mill. Environ. Sustain. 2, 75–87. https://doi.org/10.1007/s42398-019-00052-6.

Bagewadi, Z.K., Bhavikatti, J.S., Muddapur, U.M., Yaraguppi, D.A., Mulla, S.I., 2020a. Statistical optimization and characterization of bacterial cellulose produced by isolated thermophilic *Bacillus licheniformis* strain ZBT2. Carbohydr. Res. 491, 107979 https://doi.org/10.1016/j.carres.2020.107979.

Bagewadi, Z.K., Dsouza, V., Mulla, S.I., Deshpande, S.H., Muddapur, U.M., Yaraguppi, D. A., Reddy, V.D., Bhavikatti, J.S., More, S.S., 2020b. Structural and functional characterization of bacterial cellulose from *Enterobacter hormaechei* subsp. *steigerwaltii* strain ZKE7. Cellulose 27, 9181–9199. https://doi.org/10.1007/s10570-020-03412-2.

Bai, Y., Wu, W., 2022. The neutral protease immobilization: physical characterization of sodium alginate-chitosan gel beads. Appl. Biochem. Biotechnol. 194, 2269–2283. https://doi.org/10.1007/s12010-021-03773-9.

Bamal, D., Singh, A., Chaudhary, G., Kumar, M., Singh, M., Rani, N., Mundlia, P., Sehrawat, A.R., 2021. Silver nanoparticles biosynthesis, characterization, antimicrobial activities, applications, cytotoxicity and safety issues: an updated review. Nanomaterials 11, 2086. https://doi.org/10.3390/nano11082086.

Barale, S.S., Ghane, S.G., Sonawane, K.D., 2022. Purification and characterization of antibacterial surfactin isoforms produced by *Bacillus velezensis* SK. AMB Express 12, 7. https://doi.org/10.1186/s13568-022-01348-3.

Bedlovičová, Z., Strapáč, I., Baláž, M., Salayová, A., 2020. A brief overview on antioxidant activity determination of silver nanoparticles. Molecules 25, 3191. https://doi.org/10.3390/molecules25143191.

Bhatt, H.B., Singh, S.P., 2020. Cloning, expression, and structural elucidation of a biotechnologically potential alkaline serine protease from a newly isolated haloalkaliphilic *Bacillus lehensis* JO-26. Front. Microbiol. 11 https://doi.org/10.3389/fmicb.2020.00941.

Bolivar, J.M., Woodley, J.M., Fernandez-Lafuente, R., 2022. Is enzyme immobilization a mature discipline? Some critical considerations to capitalize on the benefits of immobilization. Chem. Soc. Rev. 51, 6251–6290. https://doi.org/10.1039/D2CS00083K.

Botteon, C.E.A., Silva, L.B., Ccana-Ccapatinta, G.V., Silva, T.S., Ambrosio, S.R., Veneziani, R.C.S., Bastos, J.K., Marcato, P.D., 2021. Biosynthesis and characterization of gold nanoparticles using Brazilian red propolis and evaluation of its antimicrobial and anticancer activities. Sci. Rep. 11, 1974. https://doi.org/10.1038/s41598-021-81281-w.

Brena, B., González-Pombo, P., Batista-Viera, F., 2013. Immobilization of Enzymes: A Literature Survey. pp. 15–31. Doi: 10.1007/978-1-62703-550-7_2.

Bryant, M.K., Schardl, C.L., Hesse, U., Scott, B., 2009. Evolution of a subtilisin-like protease gene family in the grass endophytic fungus *Epichloë festucae*. BMC Evol. Biol. 9, 168. https://doi.org/10.1186/1471-2148-9-168.

Bukhari, A., Ijaz, I., Gilani, E., Nazir, A., Zain, H., Saeed, R., Alarfaji, S.S., Hussain, S., Aftab, R., Naseer, Y., 2021. Green synthesis of metal and metal oxide nanoparticles using different plants' parts for antimicrobial activity and anticancer activity: a review article. Coatings 11, 1374. https://doi.org/10.3390/coatings11111374.

Chen, Y., Toth, E.A., Ruan, B., Choi, E.J., Simmerman, R., Chen, Y., He, Y., Wang, R., Godoy-Ruiz, R., King, H., Custer, G., Travis Gallagher, D., Rozak, D.A., Solomon, M., Muro, S., Weber, D.J., Orban, J., Fuerst, T.R., Bryan, P.N., 2021. Engineering subtilisin proteases that specifically degrade active RAS. Commun. Biol. 4, 299. https://doi.org/10.1038/s42003-021-01818-7.

Choi, Y.-J., Park, J.-H., Han, J., Kim, E., Jae-Wook, O., Lee, S., Kim, J.-H., Gurunathan, S., 2016. Differential cytotoxic potential of silver nanoparticles in human ovarian cancer cells and ovarian cancer stem cells. Int. J. Mol. Sci. 17, 2077. https://doi.org/10.3390/ijms17122077.

Chojniak-Gronek, J.M., Jaïowiecki, Ł., Pïaza, G.A., 2022. Bioeffects of silver nanoparticles (AgNPs) synthesized by producer of biosurfactant *Bacillus subtilis* strain: *in vitro* cytotoxicity, antioxidant properties and metabolic activities of mammalian cells. Arch. Environ. Prot. 48, 45–52. Doi: 10.24425/aep.2022.143708.

Costa, S., Azevedo, H., Reis, R., 2004. Enzyme Immobilization in Biodegradable Polymers for Biomedical Applications, in: Biodegradable Systems in Tissue Engineering and Regenerative Medicine. CRC Press. Doi: 10.1201/9780203491232.ch17.

Couto, M.T.T. do, Silva, A.V. da, Sobral, R.V.D.S., Rodrigues, C.H., Cunha, M.N.C. da, Leite, A.C.L., Figueiredo, M. do V.B., de Paula Oliveira, J., Costa, R.M.P.B., Conniff, A.E.S., Porto, A.L.F., Nascimento, T.P., 2022. Production, extraction and characterization of a serine protease with fibrinolytic, fibrinogenolytic and thrombolytic activity obtained by *Paenibacillus graminis*. Process Biochem. 118, 335–345. Doi: 10.1016/j.procbio.2022.05.005.

Danilova, I., Sharipova, M., 2020. The practical potential of *Bacilli* and their enzymes for industrial production. Front. Microbiol. 11 https://doi.org/10.3389/fmicb.2020.01782.

Das, S., Das, J., Samadder, A., Bhattacharyya, S.S., Das, D., Khuda-Bukhsh, A.R., 2013. Biosynthesized silver nanoparticles by ethanolic extracts of *Phytolacca decandra, Gelsemium sempervirens, Hydrastis canadensis* and *Thuja occidentalis* induce differential cytotoxicity through G2/M arrest in A375 cells. Colloids Surf. B Biointerfaces 101, 325–336. https://doi.org/10.1016/j.colsurfb.2012.07.008.

Ding, Y., Yang, Y., Ren, Y., Xia, J., Liu, F., Li, Y., Tang, X.-F., Tang, B., 2020. Extracellular production, characterization, and engineering of a polyextremotolerant subtilisin-like protease from feather-degrading *Thermoactinomyces vulgaris* Strain CDF. Front. Microbiol. 11 https://doi.org/10.3389/fmicb.2020.605771.

Dreaden, E.C., Alkilany, A.M., Huang, X., Murphy, C.J., El-Sayed, M.A., 2012. The golden age: gold nanoparticles for biomedicine. Chem. Soc. Rev. 41, 2740–2779. https://doi.org/10.1039/C1CS15237H.

Elizabeth, M.K., Devi, R.U., Raja, K.P., Krishna, K.B., 2022. Synthesis of phyto based metal nanoparticles: a green approach. J. Pharm. Res. Int. 20–32 https://doi.org/10.9734/jpri/2022/v34i25A35944.

Falkenberg, F., Rahba, J., Fischer, D., Bott, M., Bongaerts, J., Siegert, P., 2022. Biochemical characterization of a novel oxidatively stable, halotolerant, and high-alkaline subtilisin from Alkalihalobacillus okhensis Kh10-101 T. FEBS Open Bio 12, 1729–1746. https://doi.org/10.1002/2211-5463.13457.

Falkenberg, F., Voß, L., Bott, M., Bongaerts, J., Siegert, P., 2023. New robust subtilisins from halotolerant and halophilic *Bacillaceae*. Appl. Microbiol. Biotechnol. 107, 3939–3954. https://doi.org/10.1007/s00253-023-12553-w.

Farhadian, S., Asoodeh, A., Lagzian, M., 2015. Purification, biochemical characterization and structural modeling of a potential htrA-like serine protease from *Bacillus subtilis* DR8806. J. Mol. Catal. B Enzym. 115, 51–58. https://doi.org/10.1016/j.molcatb.2015.02.001.

Fazaa, S.A., 2022. Eco-friendly synthesis of zinc oxide nanoparticles using *Bacillus Subtilis*, characterization and antibacterial potential against *Staphylococcus aureus* associated with cardiac catheterization. Iran. J. Catal. 12, 159–168. https://doi.org/10.30495/ijc.2022.692257.

Fouad, H., Hongjie, L., Yanmei, D., Baoting, Y., El-Shakh, A., Abbas, G., Jianchu, M., 2017. Synthesis and characterization of silver nanoparticles using *Bacillus amyloliquefaciens* and Bacillus subtilis to control filarial vector *Culex pipiens pallens* and its antimicrobial activity. Artif. Cells, Nanomedicine, Biotechnol. 45, 1369–1378. https://doi.org/10.1080/21691401.2016.1241793.

Frias, J., Toubarro, D., Fraga, A., Botelho, C., Teixeira, J., Pedrosa, J., Simões, N., 2021. Purification and characterization of a thrombolytic enzyme produced by a new strain of *Bacillus subtil*. J. Microbiol. Biotechnol. 31, 327–337. https://doi.org/10.4014/jmb.2008.08010.

Furhan, J., Awasthi, P., Sharma, S., 2019. Biochemical characterization and homology modelling of cold-active alkophilic protease from Northwestern Himalayas and its application in detergent industry. Biocatal. Agric. Biotechnol. 17, 726–735. https://doi.org/10.1016/j.bcab.2019.01.028.

Gehrke, I., Geiser, A., Somborn-Schulz, A., 2015. Innovations in nanotechnology for water treatment. Nanotechnol. Sci. Appl. 8, 1–17. https://doi.org/10.2147/NSA.S43773.

George, M., Abraham, T.E., 2006. Polyionic hydrocolloids for the intestinal delivery of protein drugs: alginate and chitosan — a review. J. Control. Release 114, 1–14. https://doi.org/10.1016/j.jconrel.2006.04.017.

Glomm, W.R., Wubshet, S.G., Lindberg, D., Dankel, K.R., Afseth, N.K., Stenstad, P.M., Johnsen, H., 2021. Immobilized protease on magnetic particles for enzymatic protein hydrolysis of poultry by-products. LWT 152, 112327. https://doi.org/10.1016/j.lwt.2021.112327.

Gomaa, E.Z., 2019. Synergistic antibacterial efficiency of bacteriocin and silver nanoparticles produced by probiotic *Lactobacillus paracasei* against multidrug resistant bacteria. Int. J. Pept. Res. Ther. 25, 1113–1125. https://doi.org/10.1007/s10989-018-9759-9.

Greeshma, B.C., Mahesh, M., 2019. Biosynthesis of selenium nanoparticles from *Bacillus species* and its applications. J. Appl. Nat. Sci. 11, 810–815. https://doi.org/10.31018/jans.v11i4.2188.

Guilger-Casagrande, M., Germano-Costa, T., Bilesky-José, N., Pasquoto-Stigliani, T., Carvalho, L., Fraceto, L.F., de Lima, R., 2021. Influence of the capping of biogenic silver nanoparticles on their toxicity and mechanism of action towards *Sclerotinia sclerotiorum*. J. Nanobiotechnol. 19, 53. https://doi.org/10.1186/s12951-021-00797-5.

Guleria, S., Walia, A., Chauhan, A., Shirkot, C.K., 2016. Immobilization of *Bacillus amyloliquefaciens* SP1 and its alkaline protease in various matrices for effective hydrolysis of casein. 3 Biotech 6, 208. https://doi.org/10.1007/s13205-016-0519-2.

Gulmez, C., Atakisi, O., Dalginli, K.Y., Atakisi, E., 2018. A novel detergent additive: organic solvent- and thermo-alkaline-stable recombinant subtilisin. Int. J. Biol. Macromol. 108, 436–443. https://doi.org/10.1016/j.ijbiomac.2017.11.133.

Gurunathan, R., Huang, B., Ponnusamy, V.K., Hwang, J.-S., Dahms, H.-U., 2021. Novel recombinant keratin degrading subtilisin like serine alkaline protease from *Bacillus cereus* isolated from marine hydrothermal vent crabs. Sci. Rep. 11, 12007. https://doi.org/10.1038/s41598-021-90375-4.

Gurunathan, S., Jeong, J.-K., Han, J.W., Zhang, X.-F., Park, J.H., Kim, J.-H., 2015. Multidimensional effects of biologically synthesized silver nanoparticles in Helicobacter pylori, Helicobacter felis, and human lung (L132) and lung carcinoma A549 cells. Nanoscale Res. Lett. 10, 35. https://doi.org/10.1186/s11671-015-0747-0.

Hadjidj, R., Badis, A., Mechri, S., Eddouaouda, K., Khelouia, L., Annane, R., El Hattab, M., Jaouadi, B., 2018. Purification, biochemical, and molecular characterization of novel protease from *Bacillus licheniformis* strain K7A. Int. J. Biol. Macromol. 114, 1033–1048. https://doi.org/10.1016/j.ijbiomac.2018.03.167.

Hassan, M.E., Yang, Q., Xiao, Z., Liu, L., Wang, N., Cui, X., Yang, L., 2019. Impact of immobilization technology in industrial and pharmaceutical applications. 3 Biotech 9, 440. https://doi.org/10.1007/s13205-019-1969-0.

Hola, K., Markova, Z., Zoppellaro, G., Tucek, J., Zboril, R., 2015. Tailored functionalization of iron oxide nanoparticles for MRI, drug delivery, magnetic separation and immobilization of biosubstances. Biotechnol. Adv. 33, 1162–1176. https://doi.org/10.1016/j.biotechadv.2015.02.003.

Holyavka, M., Faizullin, D., Koroleva, V., Olshannikova, S., Zakhartchenko, N., Zuev, Y., Kondratyev, M., Zakharova, E., Artyukhov, V., 2021. Novel biotechnological formulations of cysteine proteases, immobilized on chitosan. Structure, stability and activity. Int. J. Biol. Macromol. 180, 161–176. https://doi.org/10.1016/j.ijbiomac.2021.03.016.

Hosseini-Koupaei, M., Shareghi, B., Saboury, A.A., Davar, F., Sirotkin, V.A., Hosseini-Koupaei, M.H., Enteshari, Z., 2019. Catalytic activity, structure and stability of proteinase K in the presence of biosynthesized CuO nanoparticles. Int. J. Biol. Macromol. 122, 732–744. https://doi.org/10.1016/j.ijbiomac.2018.11.001.

Hussain, F., Kamal, S., Rehman, S., Azeem, M., Bibi, I., Ahmed, T., Iqbal, H.M.N., 2017. Alkaline protease production using response surface methodology, characterization and industrial exploitation of alkaline protease of *Bacillus subtilis* sp. Catal. Lett. 147, 1204–1213. https://doi.org/10.1007/s10562-017-2017-5.

Ibrahim, H.M.M., 2018. Characterization of biosurfactants produced by novel strains of *Ochrobactrum anthropi* HM-1 and *Citrobacter freundii* HM-2 from used engine oil-contaminated soil. Egypt. J. Pet. 27, 21–29. https://doi.org/10.1016/j.ejpe.2016.12.005.

Ibrahim, S., Ahmad, Z., Manzoor, M.Z., Mujahid, M., Faheem, Z., Adnan, A., 2021b. Optimization for biogenic microbial synthesis of silver nanoparticles through response surface methodology, characterization, their antimicrobial, antioxidant, and catalytic potential. Sci. Rep. 11, 770. https://doi.org/10.1038/s41598-020-80805-0.

Ibrahim, A.S.S., Elbadawi, Y.B., El-Toni, A.M., Almaary, K.S., El-Tayeb, M.A., Elagib, A. A., Maany, D.A.F., 2021a. Stabilization and improved properties of *Salipaludibacillus agaradhaerens* alkaline protease by immobilization onto double mesoporous core-shell nanospheres. Int. J. Biol. Macromol. 166, 557–566. https://doi.org/10.1016/j.ijbiomac.2020.10.213.

Iqbal, S., Sivaraj, C., Gunasekaran, K., 2017. Antioxidant and anticancer activities of methanol extract of seeds of *Datura stramonium* l. Free Radicals Antioxidants 7, 184–189. https://doi.org/10.5530/fra.2017.2.28.

Ismail, N., Sahimi, S.N., 2021. Optimization of immobilization condition of protease extracted from silver catfish (Pangasius Sutchi) viscera in calcium alginate by using response surface methodology (RSM). Sci. Res. J. 18, 179. https://doi.org/10.24191/srj.v18i1.11754.

Jan, H., Zaman, G., Usman, H., Ansir, R., Drouet, S., Gigliolo-Guivarc'h, N., Hano, C., Abbasi, B.H., 2021. Biogenically proficient synthesis and characterization of silver nanoparticles (Ag-NPs) employing aqueous extract of Aquilegia pubiflora along with their in vitro antimicrobial, anti-cancer and other biological applications. J. Mater. Res. Technol. 15, 950–968. https://doi.org/10.1016/j.jmrt.2021.08.048.

Javed, R., Zia, M., Naz, S., Aisida, S.O., Ain, N. ul, Ao, Q., 2020. Role of capping agents in the application of nanoparticles in biomedicine and environmental remediation: recent trends and future prospects. J. Nanobiotechnol. 18, 172. https://doi.org/10.1186/s12951-020-00704-4.

Jeyabharathi, S., Naveenkumar, S., Chandramohan, S., Venkateshan, N., Gawwad, M.R. A., Elshikh, M.S., Rasheed, R.A., Al Farraj, D.A., Muthukumaran, A., 2022. Biological synthesis of zinc oxide nanoparticles from the plant extract, *Wattakaka volubilis* showed anti-microbial and anti-hyperglycemic effects. J. King Saud Univ. - Sci. 34, 101881 https://doi.org/10.1016/j.jksus.2022.101881.

Joshi, N., Kocher, G.S., Kalia, A., Banga, H.S., 2020. Development of nano-silver alkaline protease bio-conjugate depilating eco-benign formulation by utilizing potato peel based medium. Int. J. Biol. Macromol. 152, 261–271. https://doi.org/10.1016/j.ijbiomac.2020.02.251.

Kabeerdass, N., Al Otaibi, A., Rajendran, M., Manikandan, A., Kashmery, H.A., Rahman, M.M., Madhu, P., Khan, A., Asiri, A.M., Mathanmohun, M., 2021. *Bacillus*-Mediated silver nanoparticle synthesis and its antagonistic activity against bacterial and fungal pathogens. Antibiotics 10, 1334. https://doi.org/10.3390/antibiotics10111334.

Kandasamy, S., Duraisamy, S., Chinnappan, S., Balakrishnan, S., Thangasamy, S., Muthusamy, G., Arumugam, S., Palanisamy, S., 2018. Molecular modeling and docking of protease from *Bacillus* sp. for the keratin degradation. Biocatal. Agric. Biotechnol. 13, 95–104. https://doi.org/10.1016/j.bcab.2017.11.016.

Karim, A., Nawaz, M.A., Aman, A., Ul Qader, S.A., 2017. Role of anionic polysaccharide (alginate) on activity, stability and recycling efficiency of bacterial endo (1→4) β-d-glucanase of GH12 family. Catal. Letters 147, 1792–1801. https://doi.org/10.1007/s10562-017-2074-9.

Karpenko, D.V., Kanaev, S.A., 2021. Effect of nickel oxide nanoparticles on protease activity in brewing industry. IOP Conf. Ser. Earth Environ. Sci. 845, 012110 https://doi.org/10.1088/1755-1315/845/1/012110.

Kerouaz, B., Jaouadi, B., Brans, A., Saoudi, B., Habbeche, A., Haberra, S., Belghith, H., Gargroui, A., Ladjama, A., 2021. Purification and biochemical characterization of two novel extracellular keratinases with feather-degradation and hide-dehairing potential. Process Biochem. 106, 137–148. https://doi.org/10.1016/j.procbio.2021.04.009.

Khan, M.F., Kundu, D., Hazra, C., Patra, S., 2019. A strategic approach of enzyme engineering by attribute ranking and enzyme immobilization on zinc oxide nanoparticles to attain thermostability in mesophilic *Bacillus subtilis* lipase for detergent formulation. Int. J. Biol. Macromol. 136, 66–82. https://doi.org/10.1016/j.ijbiomac.2019.06.042.

Krishnamurthy, A., Belur, P.D., 2018. A novel fibrinolytic serine metalloprotease from the marine *Serratia marcescens* subsp. *sakuensis:* Purification and characterization. Int. J. Biol. Macromol. 112, 110–118. https://doi.org/10.1016/j.ijbiomac.2018.01.129.

Li, G., Liu, X., Cong, S., Deng, Y., Zheng, X., 2021. A novel serine protease with anticoagulant and fibrinolytic activities from the fruiting bodies of mushroom *Agrocybe aegerita*. Int. J. Biol. Macromol. 168, 631–639. https://doi.org/10.1016/j.ijbiomac.2020.11.118.

Li, Z., Scott, K., Hemar, Y., Zhang, H., Otter, D., 2018. Purification and characterisation of a protease (tamarillin) from tamarillo fruit. Food Chem. 256, 228–234. https://doi.org/10.1016/j.foodchem.2018.02.091.

Li, X., Zhang, S., Zhang, Q., Gan, L., Jiang, G., Tian, Y., Shi, B., 2022. Characterization and application of a novel halotolerant protease with no collagenase activity for cleaner dehairing of goatskin. Process Biochem. 113, 203–215. https://doi.org/10.1016/j.procbio.2022.01.006.

Maghraby, Y.R., El-Shabasy, R.M., Ibrahim, A.H., Azzazy, H.-M.-E.-S., 2023. Enzyme immobilization technologies and industrial applications. ACS Omega 8, 5184–5196. https://doi.org/10.1021/acsomega.2c07560.

Marathe, S.K., Vashistht, M.A., Prashanth, A., Parveen, N., Chakraborty, S., Nair, S.S., 2018. Isolation, partial purification, biochemical characterization and detergent compatibility of alkaline protease produced by Bacillus subtilis, Alcaligenes faecalis and Pseudomonas aeruginosa obtained from sea water samples. J. Genet. Eng. Biotechnol. 16, 39–46. https://doi.org/10.1016/j.jgeb.2017.10.001.

Masi, C., Chandramohan, C., Ahmed, M.F., 2018. Immobilization of the magnetic nanoparticles with alkaline protease enzyme produced by *Enterococcus hirae* and *Pseudomonas aeruginosa* Isolated from dairy effluents. Brazilian Arch. Biol. Technol. 60 https://doi.org/10.1590/1678-4324-2017160572.

Matkawala, F., Nighojkar, S., Kumar, A., Nighojkar, A., 2019. Enhanced production of alkaline protease by *Neocosmospora* sp. N1 using custard apple seed powder as inducer and its application for stain removal and dehairing. Biocatal. Agric. Biotechnol. 21, 101310 https://doi.org/10.1016/j.bcab.2019.101310.

Mechri, S., Bouacem, K., Zaraî Jaouadi, N., Rekik, H., Ben Elhoul, M., Omrane Benmrad, M., Hacene, H., Bejar, S., Bouanane-Darenfed, A., Jaouadi, B., 2019. Identification of a novel protease from the thermophilic *Anoxybacillus kamchatkensis* M1V and its application as laundry detergent additive. Extremophiles 23, 687–706. https://doi.org/10.1007/s00792-019-01123-6.

Mechri, S., Zaraî Jaouadi, N., Bouacem, K., Allala, F., Bouraoui, A., Ferard, C., Rekik, H., Noiriel, A., Abousalham, A., Bouanane-Darenfed, A., Hacène, H., Lederer, F., Baciou, L., Jaouadi, B., 2021. Cloning and heterologous expression of subtilisin SAPN, a serine alkaline protease from *Melghiribacillus thermohalophilus* Nari2AT in Escherichia coli and Pichia pastoris. Process Biochem. 105, 27–41. https://doi.org/10.1016/j.procbio.2021.03.020.

Mechri, S., Allala, F., Bouacem, K., Hasnaoui, I., Gwaithan, H., Chalbi, T.B., Saalaoui, E., Asehraou, A., Noiriel, A., Abousalham, A., Hacene, H., Bouanane-Darenfed, A., Le Roes-Hill, M., Jaouadi, B., 2022. Preparation, characterization, immobilization, and molecular docking analysis of a novel detergent-stable subtilisin-like serine protease from *Streptomyces mutabilis* strain TN-X30. Int. J. Biol. Macromol. 222, 1326–1342. https://doi.org/10.1016/j.ijbiomac.2022.09.161.

Meena, K.R., Dhiman, R., Singh, K., Kumar, S., Sharma, A., Kanwar, S.S., Mondal, R., Das, S., Franco, O.L., Mandal, A.K., 2021. Purification and identification of a surfactin biosurfactant and engine oil degradation by *Bacillus velezensis* KLP2016. Microb. Cell Fact. 20, 26. https://doi.org/10.1186/s12934-021-01519-0.

Milanezi, F.G., Meireles, L.M., de Christo Scherer, M.M., de Oliveira, J.P., da Silva, A.R., de Araujo, M.L., Endringer, D.C., Fronza, M., Guimarães, M.C.C., Scherer, R., 2019. Antioxidant, antimicrobial and cytotoxic activities of gold nanoparticles capped with

quercetin. Saudi Pharm. J. 27, 968–974. https://doi.org/10.1016/j.jsps.2019.07.005.
Mohamad, N.R., Marzuki, N.H.C., Buang, N.A., Huyop, F., Wahab, R.A., 2015. An overview of technologies for immobilization of enzymes and surface analysis techniques for immobilized enzymes. Biotechnol. Biotechnol. Equip. 29, 205–220. https://doi.org/10.1080/13102818.2015.1008192.
Mohammadi, M., Ashjari, M., Dezvarei, S., Yousefi, M., Babaki, M., Mohammadi, J., 2015. Rapid and high-density covalent immobilization of *Rhizomucor miehei* lipase using a multi component reaction: application in biodiesel production. RSC Adv. 5, 32698–32705. https://doi.org/10.1039/C5RA03299G.
Mohd Hussin, F.N.N., Attan, N., Wahab, R.A., 2020. Taguchi design-assisted immobilization of *Candida rugosa* lipase onto a ternary alginate/nanocellulose/montmorillonite composite: physicochemical characterization, thermal stability and reusability studies. Enzyme Microb. Technol. 136, 109506 https://doi.org/10.1016/j.enzmictec.2019.109506.
Mokashe, N., Chaudhari, B., Patil, U., 2018. Operative utility of salt-stable proteases of halophilic and halotolerant bacteria in the biotechnology sector. Int. J. Biol. Macromol. 117, 493–522. https://doi.org/10.1016/j.ijbiomac.2018.05.217.
Muhammed, N.S., Hussin, N., Lim, A.S., Jonet, M.A., Mohamad, S.E., Jamaluddin, H., 2021. Recombinant production and characterization of an extracellular subtilisin-like serine protease from *Acinetobacter baumannii* of fermented food origin. Protein J. 40, 419–435. https://doi.org/10.1007/s10930-021-09986-5.
Mukherjee, A.K., Rai, S.K., Thakur, R., Chattopadhyay, P., Kar, S.K., 2012. Bafibrinase: A non-toxic, non-hemorrhagic, direct-acting fibrinolytic serine protease from *Bacillus* sp. strain AS-S20-I exhibits *in vivo* anticoagulant activity and thrombolytic potency. Biochimie 94, 1300–1308. https://doi.org/10.1016/j.biochi.2012.02.027.
Nadeem, F., Mehmood, T., Naveed, M., Shamas, S., Saman, T., Anwar, Z., 2020. Protease production from *Cheotomium globusum* through central composite design using agricultural wastes and its immobilization for industrial exploitation. Waste Biomass Valorization 11, 6529–6539. https://doi.org/10.1007/s12649-019-00890-9.
Naseem, T., Durrani, T., 2021. The role of some important metal oxide nanoparticles for wastewater and antibacterial applications: a review. Environ. Chem. Ecotoxicol. 3, 59–75. https://doi.org/10.1016/j.enceco.2020.12.001.
Nelson Ademakinwa, A., Adenike Ayinla, Z., Kayode Agboola, F., 2021. Fungal α-amylase entrapped in agar-agar organic matrix "beads" enhances fabric starch-desizing potentials and α-amylase-detergent compatibility, pp. 1–19.
Nina Vanessa, W.D., Laurette Blandine, M.K., Jong, N.E., 2022. Inclusion of partly purified protease from *Abrus precatorius* Linn in Ca-alginate gel beads. Heliyon 8, e11791.
Omole, R.K., Torimiro, N., Alayande, S.O., Ajenifuja, E., 2018. Silver nanoparticles synthesized from *Bacillus subtilis* for detection of deterioration in the post-harvest spoilage of fruit. Sustain. Chem. Pharm. 10, 33–40. https://doi.org/10.1016/j.scp.2018.08.005.
Oshi, M.A., Haider, A., Siddique, M.I., Zeb, A., Jamal, S.B., Khalil, A.A.K., Naeem, M., 2022. Nanomaterials for chronic inflammatory diseases: the current status and future prospects. Appl. Nanosci. 12, 3097–3110. https://doi.org/10.1007/s13204-021-02019-8.
Özbek, B., Ünal, Ş., 2017. Preparation and characterization of polymer-coated mesoporous silica nanoparticles and their application in Subtilisin immobilization. Korean J. Chem. Eng. 34, 1992–2001. https://doi.org/10.1007/s11814-017-0045-x.
P, M., Moopantakath, J., Imchen, M., Kumavath, R., SenthilKumar, P.K., 2021. Identification of Multi-Potent Protein Subtilisin A from halophilic bacterium *Bacillus firmus* VE2. Microb. Pathog. 157, 105007. Doi: 10.1016/j.micpath.2021.105007.
Padilha, G.S., Tambourgi, E.B., Alegre, R.M., 2018. Evaluation of lipase from Burkholderia cepacia immobilized in alginate beads and application in the synthesis of banana flavor (isoamyl acetate). Chem. Eng. Commun. 205, 23–33. https://doi.org/10.1080/00986445.2017.1370707.
Patra, J.K., Das, G., Fraceto, L.F., Vangelie, E., Campos, R., Rodriguez, P., Susana, L., Torres, A., Armando, L., Torres, D., Grillo, R., 2018. Nano based drug delivery systems : recent developments and future prospects. J. Nanobiotechnol. 1–33 https://doi.org/10.1186/s12951-018-0392-8.
Patra, S., Mukherjee, S., Barui, A.K., Ganguly, A., Sreedhar, B., Patra, C.R., 2015. Green synthesis, characterization of gold and silver nanoparticles and their potential application for cancer therapeutics. Mater. Sci. Eng. C 53, 298–309. https://doi.org/10.1016/j.msec.2015.04.048.
Pawar, V.A., Prajapati, A.S., Akhani, R.C., Patel, D.H., Subramanian, R.B., 2018. Molecular and biochemical characterization of a thermostable keratinase from *Bacillus altitudinis* RBDV1. 3 Biotech 8, 107. https://doi.org/10.1007/s13205-018-1130-5.
Pele, M.A., Ribeaux, D.R., Vieira, E.R., Souza, A.F., Luna, M.A.C., Rodríguez, D.M., Andrade, R.F.S., Alviano, D.S., Alviano, C.S., Barreto-Bergter, E., Santiago, A.L.C.M. A., Campos-Takaki, G.M., 2019. Conversion of renewable substrates for biosurfactant production by *Rhizopus arrhizus* UCP 1607 and enhancing the removal of diesel oil from marine soil. Electron. J. Biotechnol. 38, 40–48. https://doi.org/10.1016/j.ejbt.2018.12.003.
Peng, Y., Yang, X.-J., Xiao, L., Zhang, Y.-Z., 2004. Cloning and expression of a fibrinolytic enzyme (subtilisin DFE) gene from Bacillus amyloliquefaciens DC-4 in Bacillus subtilis. Res. Microbiol. 155, 167–173. https://doi.org/10.1016/j.resmic.2003.10.004.
Pereira de Sousa, I., Cattoz, B., Wilcox, M.D., Griffiths, P.C., Dalgliesh, R., Rogers, S., Bernkop-Schnürch, A., 2015. Nanoparticles decorated with proteolytic enzymes, a promising strategy to overcome the mucus barrier. Eur. J. Pharm. Biopharm. 97, 257–264. https://doi.org/10.1016/j.ejpb.2015.01.008.
Poomtien, J., Thaniyavarn, J., Pinphanichakarn, P., Jindamorakot, S., Morikawa, M., 2013. Production and characterization of a biosurfactant from *Cyberlindnera samutprakarnensis* JP52 T. Biosci. Biotechnol. Biochem. 77, 2362–2370. https://doi.org/10.1271/bbb.130434.
Prabhawathi, V., Sivakumar, P.M., Boobalan, T., Manohar, C.M., Doble, M., 2019. Design of antimicrobial polycaprolactam nanocomposite by immobilizing subtilisin conjugated Au/Ag core-shell nanoparticles for biomedical applications. Mater. Sci. Eng. C 94, 656–665. https://doi.org/10.1016/j.msec.2018.10.020.
Priyanka, P., Kinsella, G.K., Henehan, G.T., Ryan, B.J., 2019. The effect of calcium alginate entrapment on the stability of novel lipases from P. Reinekei and *P. brenneri*. Trends Pept. Protein Sci. 4, 1–10 (e7).
Qamar, S.A., Asgher, M., Bilal, M., 2020. Immobilization of Alkaline Protease From *Bacillus brevis* Using Ca-Alginate Entrapment Strategy for Improved Catalytic Stability, Silver Recovery, and Dehairing Potentialities. Catal. Lett. 150, 3572–3583. https://doi.org/10.1007/s10562-020-03268-y.
Radini, I.A., Hasan, N., Malik, M.A., Khan, Z., 2018. Biosynthesis of iron nanoparticles using *Trigonella foenum-graecum* seed extract for photocatalytic methyl orange dye degradation and antibacterial applications. J. Photochem. Photobiol. B Biol. 183, 154–163. https://doi.org/10.1016/j.jphotobiol.2018.04.014.
Rana, A.M., Devreese, B., De Waele, S., Sodhozai, A.R., Rozi, M., Rashid, S., Hameed, A., Ali, N., 2023. Immobilization and docking studies of Carlsberg subtilisin for application in poultry industry. PLoS One 18, e0269717.
Rozanov, A.S., Shekhovtsov, S.V., Bogacheva, N.V., Pershina, E.G., Ryapolova, A.V., Bytyak, D.S., Peltek, S.E., 2021. Production of subtilisin proteases in bacteria and yeast. Vavilov J. Genet. Breed. 25, 125–134. https://doi.org/10.18699/VJ21.015.
S.S., D., M.B., M., M.N., S.K., Golla, R., P., R.K., S., D., Hosamani, R., 2019. Antimicrobial, anticoagulant and antiplatelet activities of green synthesized silver nanoparticles using *Selaginella* (Sanjeevini) plant extract. Int. J. Biol. Macromol. 131, 787–797. Doi: 10.1016/j.ijbiomac.2019.01.222.
Salis, A., Bilaničová, D., Ninham, B.W., Monduzzi, M., 2007. Hofmeister effects in enzymatic activity: weak and strong electrolyte influences on the activity of *Candida rugosa* Lipase. J. Phys. Chem. B 111, 1149–1156. https://doi.org/10.1021/jp066346z.
Sarkar, G., K, S., 2020. Extraction and characterization of alkaline protease from *Streptomyces* sp. GS-1 and its application as dehairing agent. Biocatal. Agric. Biotechnol. 25, 101590. Doi: 10.1016/j.bcab.2020.101590.
Sattar, H., Aman, A., Qader, S.A.U., 2018. Agar-agar immobilization: An alternative approach for the entrapment of protease to improve the catalytic efficiency, thermal stability and recycling efficiency. Int. J. Biol. Macromol. 111, 917–922. https://doi.org/10.1016/j.ijbiomac.2018.01.105.
Sawetaji, S., 2023. A protease from Moringa oleifera Lam exhibits plasmin like activity of blood clot solubilization under *ex-vivo* and *in-vitro* hydrolysis of fibrin.
Schaller, A., Stintzi, A., Rivas, S., Serrano, I., Chichkova, N.V., Vartapetian, A.B., Martínez, D., Guiamét, J.J., Sueldo, D.J., van der Hoorn, R.A.L., Ramírez, V., Vera, P., 2018. From structure to function – a family portrait of plant subtilases. New Phytol. 218, 901–915. https://doi.org/10.1111/nph.14582.
Shabaani, M., Rahaiee, S., Zare, M., Jafari, S.M., 2020. Green synthesis of ZnO nanoparticles using loquat seed extract; Biological functions and photocatalytic degradation properties. LWT 134, 110133. https://doi.org/10.1016/j.lwt.2020.110133.
Sharma, C., Salem, G.E.M., Sharma, N., Gautam, P., Singh, R., 2019. Thrombolytic potential of novel thiol-dependent fibrinolytic protease from *Bacillus cereus* RSA1. Biomolecules 10, 3. https://doi.org/10.3390/biom10010003.
Sharma, R., Singh, J., Verma, N., 2018. Production, characterization and environmental applications of biosurfactants from *Bacillus amyloliquefaciens* and *Bacillus subtilis*. Biocatal. Agric. Biotechnol. 16, 132–139. https://doi.org/10.1016/j.bcab.2018.07.028.
Shettar, S.S., Bagewadi, Z.K., Kolvekar, H.N., Yunus Khan, T.M., Shamsudeen, S.M., 2023a. Optimization of subtilisin production from *Bacillus subtilis* strain ZK3 and biological and molecular characterization of synthesized subtilisin capped nanoparticles. Saudi J. Biol. Sci. 30, 103807 https://doi.org/10.1016/j.sjbs.2023.103807.
Shettar, S.S., Bagewadi, Z.K., Yaraguppi, D.A., Das, S., Mahanta, N., Singh, S.P., Katti, A., Saikia, D., 2023b. Gene expression and molecular characterization of recombinant subtilisin from *Bacillus subtilis* with antibacterial, antioxidant and anticancer properties. Int. J. Biol. Macromol. 249, 125960 https://doi.org/10.1016/j.ijbiomac.2023.125960.
Sidhu, P.K., Nehra, K., 2020. Bacteriocin-capped silver nanoparticles for enhanced antimicrobial efficacy against food pathogens. IET Nanobiotechnol. 14, 245–252. https://doi.org/10.1049/iet-nbt.2019.0323.
Sidhu, P.K., Nehra, K., 2021. Purification and characterization of bacteriocin Bac23 extracted from *Lactobacillus plantarum* PKLP5 and its interaction with silver nanoparticles for enhanced antimicrobial spectrum against food-borne pathogens. LWT 139, 110546. https://doi.org/10.1016/j.lwt.2020.110546.
Tacias-Pascacio, V.G., Morellon-Sterling, R., Castañeda-Valbuena, D., Berenguer-Murcia, Á., Kamli, M.R., Tavano, O., Fernandez-Lafuente, R., 2021. Immobilization of papain: A review. Int. J. Biol. Macromol. 188, 94–113. https://doi.org/10.1016/j.ijbiomac.2021.08.016.
Tamreihao, K., Mukherjee, S., Khunjamayum, R., Devi, L.J., Asem, R.S., Ningthoujam, D. S., 2019. Feather degradation by keratinolytic bacteria and biofertilizing potential for sustainable agricultural production. J. Basic Microbiol. 59, 4–13. https://doi.org/10.1002/jobm.201800434.
Thakrar, F.J., Singh, S.P., 2019. Catalytic, thermodynamic and structural properties of an immobilized and highly thermostable alkaline protease from a haloalkaliphilic actinobacteria, *Nocardiopsis* alba TATA-5. Bioresour. Technol. 278, 150–158. https://doi.org/10.1016/j.biortech.2019.01.058.

Thu, N.T.A., Khue, N.T.M., Huy, N.D., Tien, N.Q.D., Loc, N.H., 2020. Characterizations and fibrinolytic activity of serine protease from *Bacillus subtilis* C10. Curr. Pharm. Biotechnol. 21, 110–116. https://doi.org/10.2174/1389201020666191002145415.

Ullah, A., Yin, X., Wang, F., Xu, B.o., Mirani, Z.A., Xu, B., Chan, M.W.H., Ali, A., Usman, M., Ali, N., Naveed, M., 2021. Biosynthesis of selenium nanoparticles (via Bacillus subtilis BSN313), and their isolation, characterization, and bioactivities. Molecules 26, 5559. https://doi.org/10.3390/molecules26185559.

Wahba, M.I., 2022. Gum tragacanth for immobilization of *Bacillus licheniformis* protease: optimization, thermodynamics and application. React. Funct. Polym. 179, 105366 https://doi.org/10.1016/j.reactfunctpolym.2022.105366.

Wahba, M.I., Hassan, M.E., 2017. Agar-carrageenan hydrogel blend as a carrier for the covalent immobilization of β-D-galactosidase. Macromol. Res. 25, 913–923. https://doi.org/10.1007/s13233-017-5123-8.

Yang, S., Zhai, L., Huang, L., Meng, D., Li, J., Hao, Z., Guan, Z., Cai, Y., Liao, X., 2020. Mining of alkaline proteases from *Bacillus altitudinis* W3 for desensitization of milk proteins: their heterologous expression, purification, and characterization. Int. J. Biol. Macromol. 153, 1220–1230. https://doi.org/10.1016/j.ijbiomac.2019.10.252.

Yao, Z., Kim, J.A., Kim, J.H., 2019. Characterization of a fibrinolytic enzyme secreted by *Bacillus velezensis* BS2 isolated from sea squirt jeotgal. J. Microbiol. Biotechnol. 29, 347–356. https://doi.org/10.4014/jmb.1810.10053.

Yildirim, V., Baltaci, M.O., Ozgencli, I., Sisecioglu, M., Adiguzel, A., Adiguzel, G., 2017. Purification and biochemical characterization of a novel thermostable serine alkaline protease from *Aeribacillus pallidus* C10: a potential additive for detergents. J. Enzyme Inhib. Med. Chem. 32, 468–477. https://doi.org/10.1080/14756366.2016.1261131.

Yu, X., Li, J., Mu, D., Zhang, H., Liu, Q., Chen, G., 2021. Green synthesis and characterizations of silver nanoparticles with enhanced antibacterial properties by secondary metabolites of Bacillus subtilis (SDUM301120). Green Chem. Lett. Rev. 14, 190–203. https://doi.org/10.1080/17518253.2021.1894244.

Zhai, X., Zhang, C., Zhao, G., Stoll, S., Ren, F., Leng, X., 2017. Antioxidant capacities of the selenium nanoparticles stabilized by chitosan. J. Nanobiotechnology 15, 4. https://doi.org/10.1186/s12951-016-0243-4.

Zobaer, M., Ali, F., Anwar, M.N., Bappi, M.S.H., Bakar, T.B., Hossain, T.J., 2023. Isolation of biosurfactant producing bacteria from oil-spilled soil and characterization of their secreted biosurfactants in pathogen-inhibition and oil-emulsification. SSRN Electron J. https://doi.org/10.2139/ssrn.4320992.